A Nonlinear Model of Internal Tide Transformation on the Australian North West Shelf

PETER E. HOLLOWAY

School of Geography and Oceanography, University College, University of New South Wales, Australian Defence Force Academy, Canberra, Australia

EFIM PELINOVSKY AND TATYANA TALIPOVA

Institute of Applied Physics, Russian Academy of Science, Nizhny Novgorod, Russia

BELINDA BARNES

School of Geography and Oceanography, University College, University of New South Wales, Australian Defence Force Academy, Canberra, Australia

(Manuscript received 27 July 1995, in final form 2 May 1996)

ABSTRACT

A numerical solution to the generalized Korteweg-de Vries (K-dV) equation, including horizontal variability and dissipation, is used to model the evolution of an initially sinusoidal long internal wave, representing an internal tide. The model shows the development of the waveform to the formation of shocks and solitons as it propagates shoreward over the continental slope and shelf. The model is run using observed hydrographic conditions from the Australian North West Shelf and results are compared to current meter and thermistor observations from the shelf-break region. It is found from observations that the coefficient of nonlinearity in the K-dV equation changes sign from negative in deep water to positive in shallow water, and this plays a major role in determining the form of the internal tide transformation. On the shelf there is strong temporal variability in the nonlinear coefficient due to both background shear flow and the large amplitude of the internal tide, which distorts the density profile over a wave period. Both the model and observations show the formation of an initial shock on the leading face of the internal tide. In shallow water, the change in sign of the coefficient of nonlinearity causes the shock to evolve into a tail of short period sinusoidal waves. After further propagation a second shock forms on the back face of the wave, followed by a packet of solitons. The inclusion of bottom friction in the model is investigated along with the dependance on initial wave amplitude and variability in the coefficients of nonlinearity and dispersion. Friction is found to be important in limiting the amplitudes of the evolving waves.

1. Introduction

Internal tides, generated through the action of the barotropic tide forcing stratified water over sloping topography, are a common feature of many continental slope and shelf regions. These internal tides are long internal waves most commonly seen at semidiurnal periods (12.42 h for the M_2 constituent) and with wavelengths of tens of kilometers. In many instances, these long internal waves are observed to form instabilities seen as internal bores, short period waves, and soliton-like waves (Holloway 1987; New and Pingree 1990, 1992). These short waves have periods on the scale of ten minutes and wavelengths of hundreds of meters.

Huthnance (1989) gives a comprehensive review of internal tide observations, and Ostrovsky and Stepanyants (1989) and Jeans (1995) review internal solitary wave observations from the ocean. In most cases it appears that internal solitary waves are generated through topographic effects (sills and continental slopes) on tidal flow or on long internal waves such as internal tides. These energetic waves are important dissipation mechanisms for the long waves and provide a source of mixing energy that can move sediment (e.g., Boczar-Karakiewicz et al. 1991) or stir nutrients into the photic layers of the ocean and increase biological productivity (e.g., Sandstrom and Elliot 1984).

There have been a number of theoretical, laboratory, and numerical studies of the generation of solitons in the ocean. Most of these have considered the generation of solitons from flow over a ridge or sill, for example,

Corresponding author address: Dr. Peter E. Holloway, School of Geography and Oceanography, University College, University of New South Wales, Australian Defence Force Academy, Canberra ACT 2600, Australia.
E-mail: p-holloway@adfa.oz.au

© 1997 American Meteorological Society

Unauthenticated | Downloaded 09/25/22 05:48 AM UTC

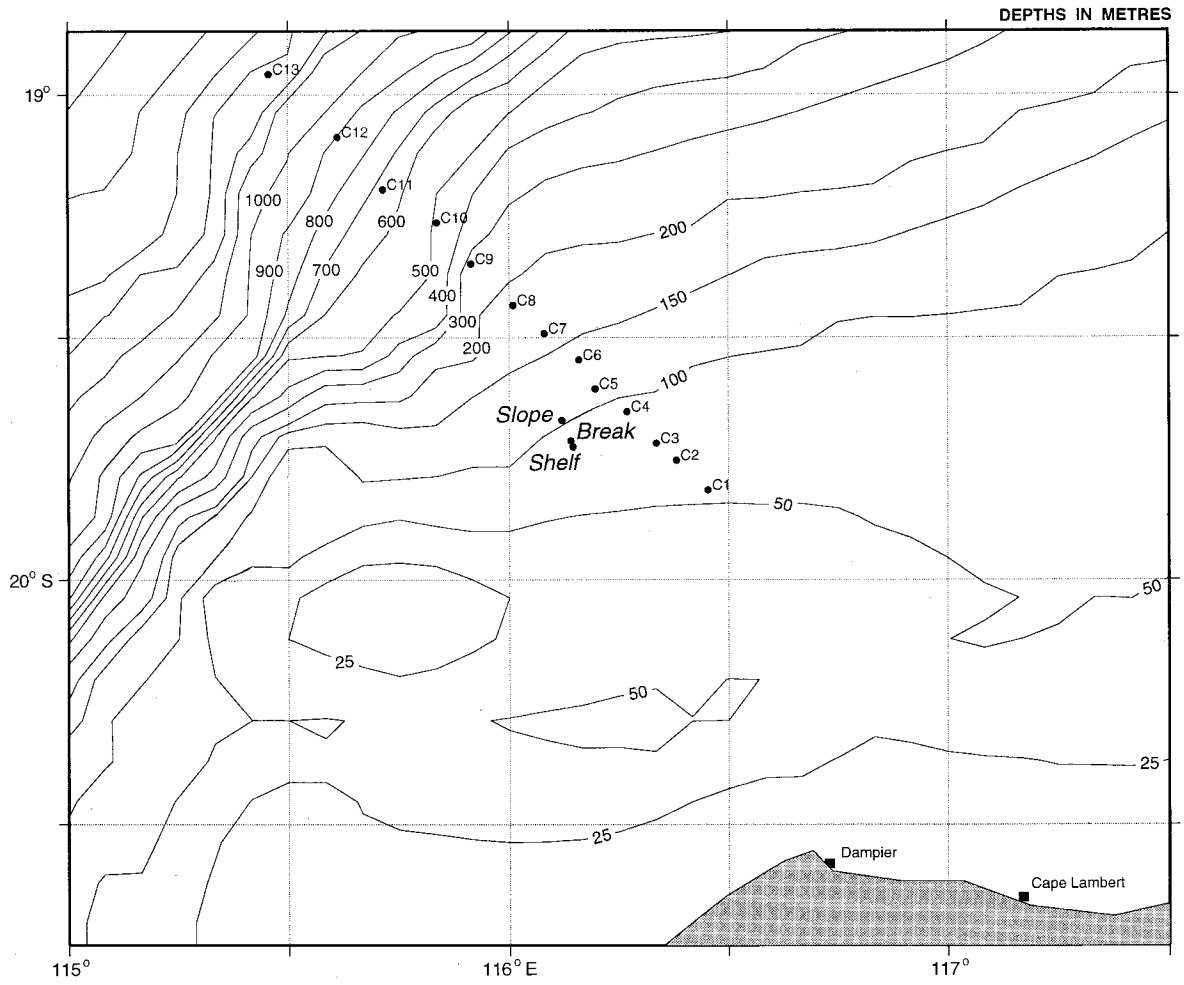

FIG. 1. Map of the Australian North West Shelf showing bathymetry, CTD station locations from 1995 (C1 to C13), and mooring locations *Slope*, *Break*, and *Shelf* from 1992.

Maxworthy (1979). Lee and Beardsley (1974) made a numerical study of solitons evolving from an initial step, and Lamb (1994) used a finite difference numerical model to investigate nonlinear wave formation from an internal tide. In this paper, a numerical solution to a Korteweg-de Vries (K-dV) equation is used to model the evolution of a shoreward propagating internal tide over the slope and shelf region. The internal tide is modeled as an initially sinusoidal waveform and also as the evolution of an observed waveform. Account is made of the effects of variable depth, dissipation, spatially variable coefficients of the K-dV equation, and the influence of background shear flow on wave properties.

2. Observations of shocks and solitons

Observations of internal tides featuring shocks, solitonlike wave forms, and short period oscillations are discussed in this section. The observations are from three moorings placed in a line across the shelf break on the Australian North West Shelf (NWS). The location of the moorings is shown in Fig. 1, and a bathymetric cross section showing the location of instruments is shown in Fig. 2. All instruments recorded both current velocity and temperature. Current meters were either Steedman acoustic current meters (sampling 2-min vector averages) or Inter Ocean ''S4'' electromagnetic current meters (sampling 1-min vector averages every 6 min).

The temperature time series data are, at each time step, linearly interpolated through the vertical to find the depth of particular isotherms. This provides a time sequence of vertical displacements associated with the internal waves. The predominant direction of propagation of the internal tide in this region is onshore, at approximately 135° east of north (Holloway 1994). The velocity records are resolved into orthogonal components and the component in the direction of the line of current meters (158°) is presented in this paper.

Figures 3a–d show example time series, for each of the three locations, of isotherm displacements (height

Unauthenticated | Downloaded 09/25/22 05:48 AM UTC

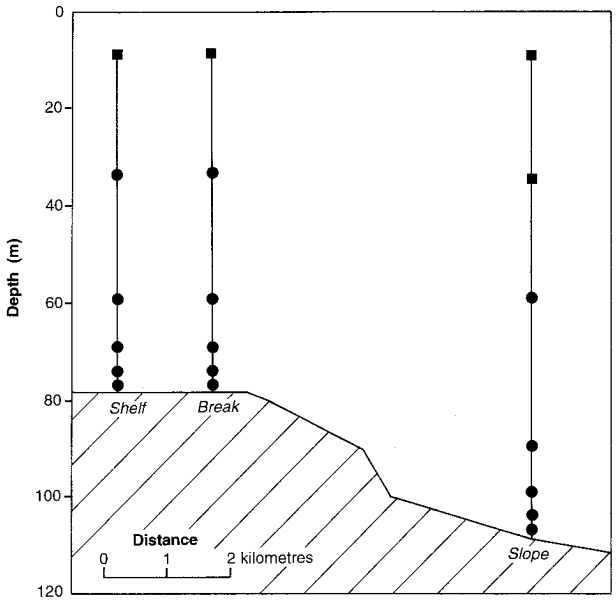

FIG. 2. Bathymetric cross section showing mooring locations and current meter positions for the 1992 dataset. Current meters were Steedman Acoustic current meters (●) or InterOcean S4 electromagnetic current meters (■).

of isotherms above the seabed) and of onshore currents at a height of 10 m above the seabed for several different time segments. The isotherm displacements are calculated by linear interpolation between the measurement depths, as shown in Fig. 1. Only the near-seabed currents are shown as, generally, the currents associated with the internal waves in this region have a maximum near the seabed. Background temperature profiles (e.g., Fig. 6) show the stratification to be characterized by continuous gradients rather than by a two-layer structure. This means that the calculated isotherm displacements are a reliable measure of the internal wave shape. This is further supported by the strong similarity between the isotherm displacement and current time series.

The first examples are seen in Fig. 3a for 27 and 28 March 1992. At the deeper *slope* mooring, relatively smooth internal tides are seen with solitons or short period oscillatory waves at the front face of the waves. By the time the internal tide has propagated the 5 km to the *break* mooring, the waves have steepened showing shocks on both the front and back faces. Large amplitude solitons are seen to develop on the front face of the wave; for example, events A_4 and A_5 show solitons of approximately 40-m height evolving between *slope* and *shelf* moorings. These waves are also seen in the onshore velocity records. However, the solitons are particularly large in the currents at the slope mooring. There is a distinct difference in the nature of the short period oscillations following the shock on the front face of the wave when comparing events A_2 to A_4 and A_5 at the slope location. For A_2 the oscillations appear as a random set of waves, whereas at the other times there are 1 to 2 solitons. Most of the solitons seen are positive, that is, an upward displacement.

The velocities associated with the internal tide are also very strong at the slope location. Maximum currents are 80 cm s^{-1} in the offshore direction, occuring just prior to the front face of the wave. After the shock and associated solitons, there is a near linear slope in velocity until the next shock occurs. The currents due to the internal tide are much weaker at the break and shelf locations indicating strong dissipation of the internal tide.

Further examples of vertical displacements and onshore velocities are seen in Fig. 3b for 31 March and 1 April 1992. Again, very steep faced shocks on both the forward and back face of the waves are seen to develop between the slope and break locations. At the shelf, near square-waves of height up to 50 m are seen (e.g., B_3 to B_4) resulting from strong shocks on both the forward and back faces of the wave.

Figure 3c for 11 April shows significantly different wave forms than the previous examples. The large waves seen at the break and shelf evolve from a quite small amplitude wave (5 to 10 m) at slope. In addition, the wave profile is covered by short period oscillations, particularly at the slope and seen in both the vertical displacements and velocity. The second oscillation at the slope (near C_2) is broken into many oscillations as it propagates to the break and there is no sharp shock. The velocities are much weaker than in the previous examples.

A similar pattern to 11 April is seen on 13 April (Fig. 3d) where a large number of short waves are seen superimposed on the longer internal tide. At D_2, large amplitude solitons (40 m) are seen to evolve from a weak shock seen at the slope. These lead solitons are followed by a large number of oscillations at both break and shelf. This is in contrast to the shocks in Figs. 3a and 3b where after very strong shocks, only a small number of solitons or short oscillations are seen. Around D_1 at both break and shelf locations, very high frequency waves are seen and they appear as a random wave field. At D_2 more ordered solitons are seen.

3. Korteweg-de Vries equation for an internal wave field

The K-dV equation is well known as an appropriate physical model for the description of the nonlinear and dispersive properties of an internal wave field (Benney 1966; Lee and Beardsley 1974; Pelinovsky et al. 1977; Maslowe and Redekopp 1980; Grimshaw 1981, 1983; Gear and Grimshaw 1983). It is derived as a perturbation expansion and is valid to first order in wave amplitude and for long waves; that is, it is assumed that $H/\lambda \ll 1$ and $a/H \ll 1$, where H is the local water depth, λ is a representative wavelength, and a is a representative wave amplitude. For arbitrary vertical stratification of

Unauthenticated | Downloaded 09/25/22 05:48 AM UTC

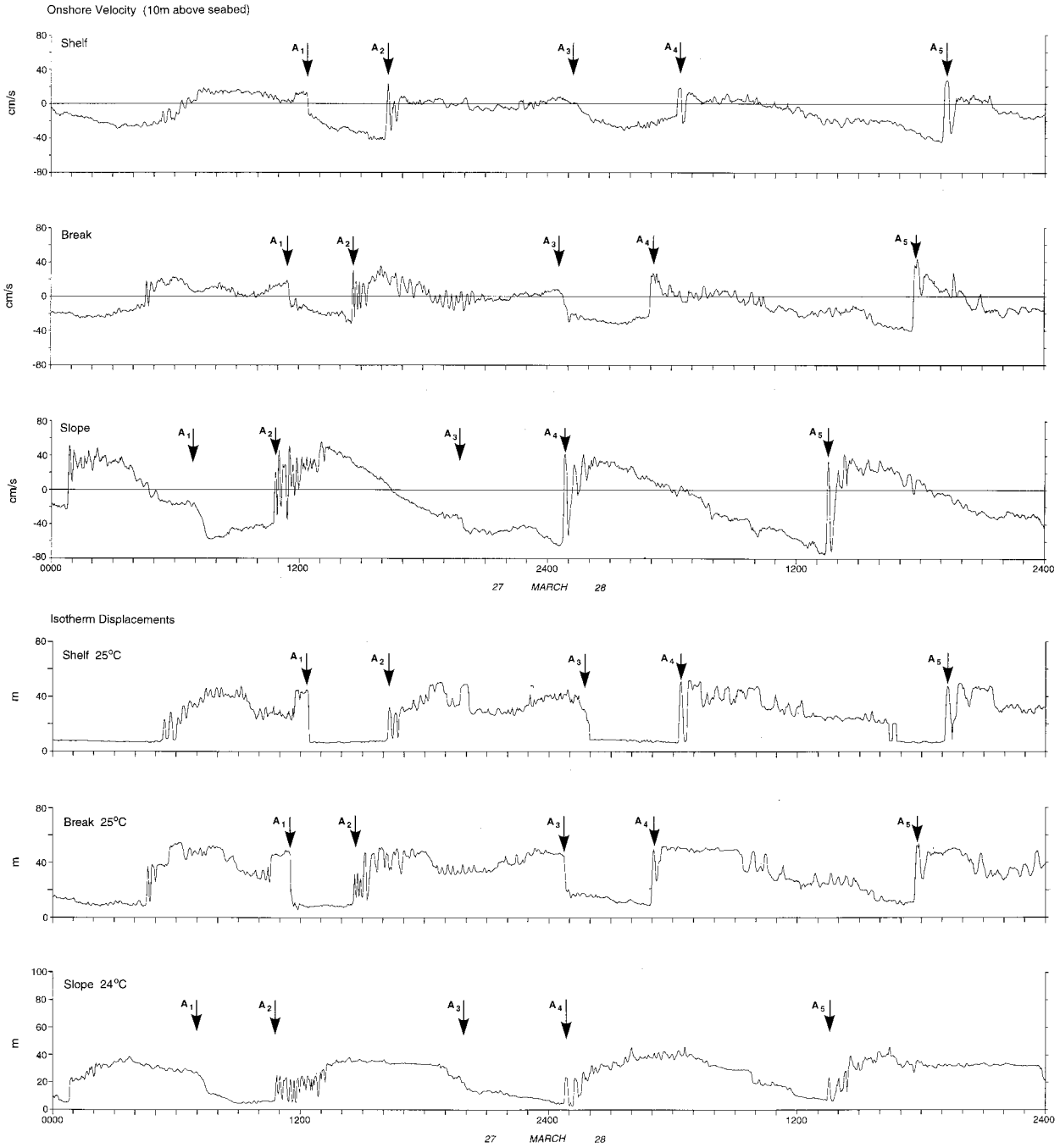

FIG. 3a. Time series of onshore velocity component measured 10 m above the seabed and isotherm displacements from the slope, break and shelf locations over the period 0000 27 to 2400 28 March 1992.

ocean density and background shear flow, the K-dV equation is written as

$$\frac{\partial \eta}{\partial t} + c\frac{\partial \eta}{\partial x} + \alpha\eta\frac{\partial \eta}{\partial x} + \beta\frac{\partial^3 \eta}{\partial x^3} = 0, \qquad (1)$$

where $\eta(x, t)$ is the vertical displacement of the pycnocline, x is the horizontal coordinate, and t is time. The parameters α, β, and c are coefficients of nonlinearity, dispersion, and phase speed of long internal waves, respectively. They are determined by the back-

Unauthenticated | Downloaded 09/25/22 05:48 AM UTC

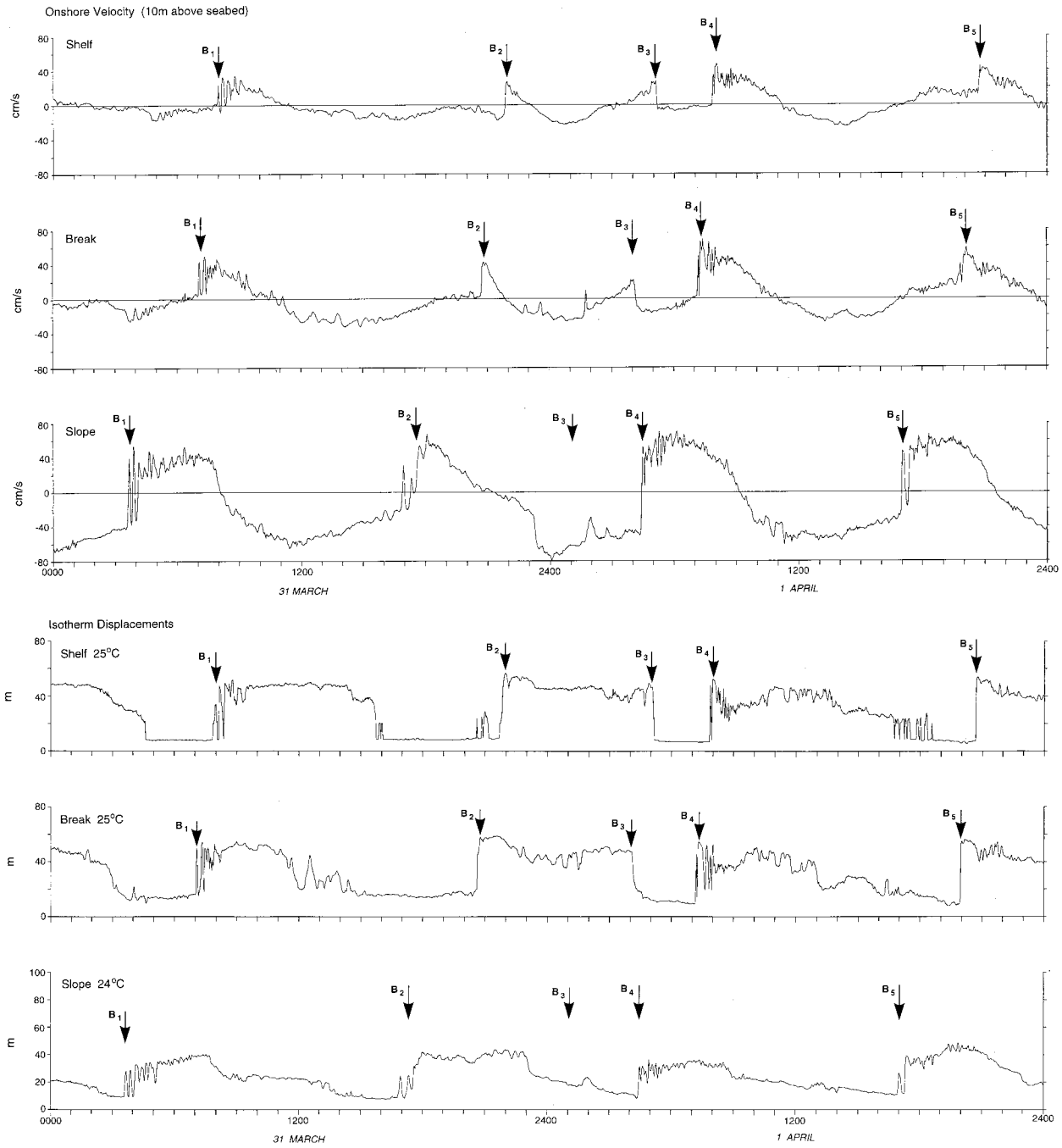

FIG. 3b. As in Fig. 3a but over the period 0000 31 March to 2400 1 April 1992.

ground density and horizontal velocity profiles and are defined as (in the Boussinesq approximation)

$$\alpha = \left(\frac{3}{2}\right)\frac{\int_{-H}^{0}(c-U)^2(d\Phi/dz)^3\,dz}{\int_{-H}^{0}(c-U)(d\Phi/dz)^2\,dz}, \qquad (2)$$

$$\beta = \left(\frac{1}{2}\right)\frac{\int_{-H}^{0}(c-U)^2\Phi^2\,dz}{\int_{-H}^{0}(c-U)(d\Phi/dz)^2\,dz}, \qquad (3)$$

where z is a vertical coordinate, positive upward. The phase speed of a linear long wave c and the vertical

Unauthenticated | Downloaded 09/25/22 05:48 AM UTC

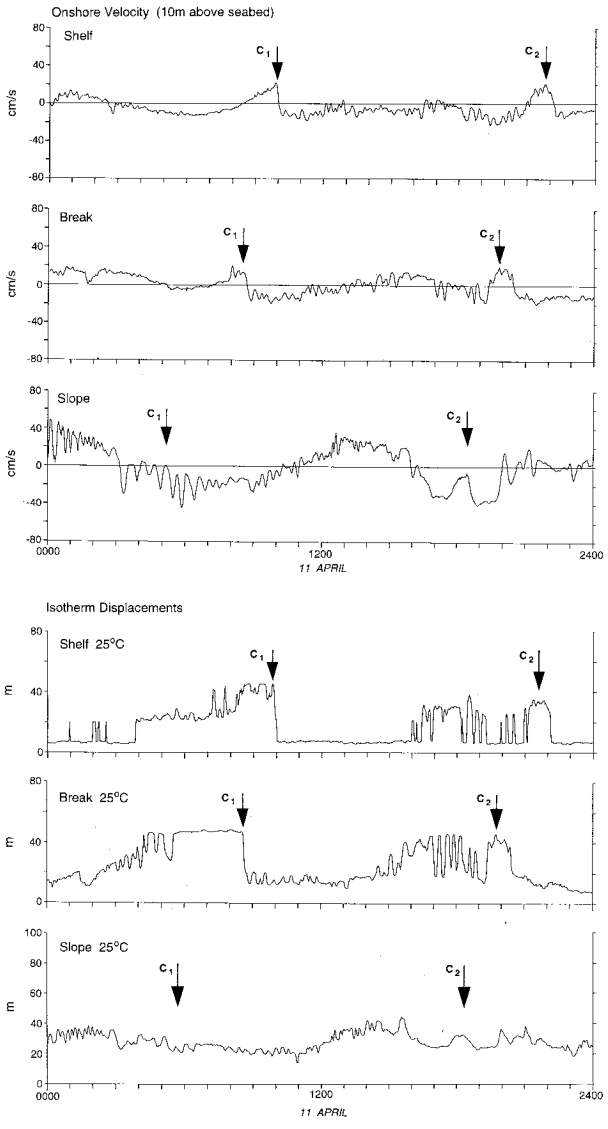

FIG. 3c. As in Fig. 3a but over the period 0000 to 2400 11 April 1992.

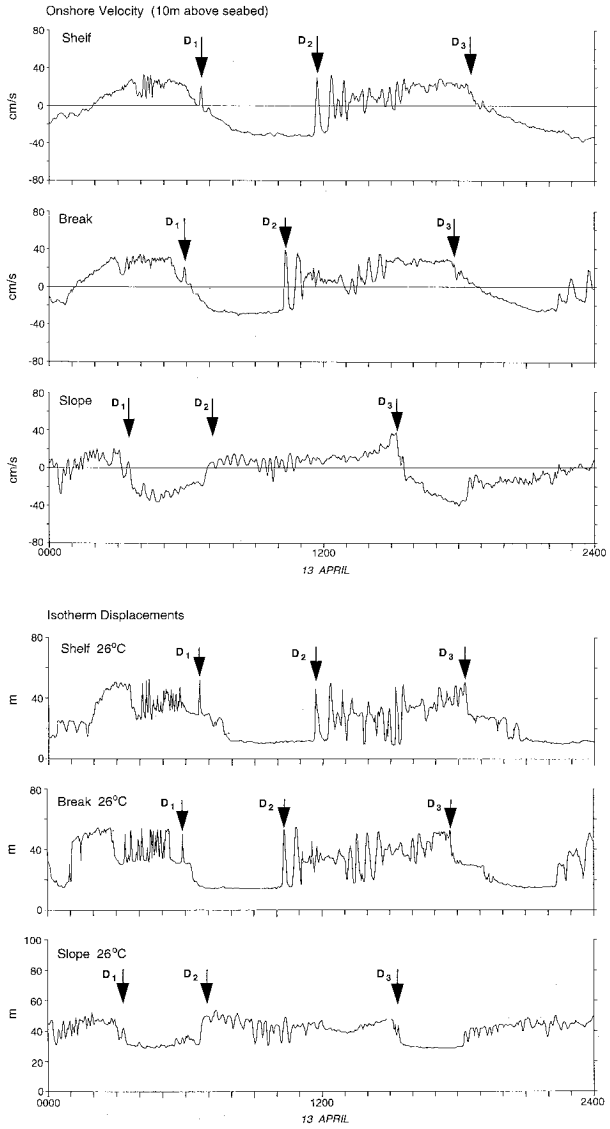

FIG. 3d. As in Fig. 3a but over the period 0000 to 2400 13 April 1992.

structure of vertical-displacement amplitude of a wave mode $\Phi(z)$ are determined by the solution of the eigenvalue problem

$$\frac{d}{dz}\left[(c - U)^2 \frac{d\Phi}{dz}\right] + N^2(z)\Phi = 0,$$

$$\Phi(-H) = \Phi(0) = 0, \qquad (4)$$

where $N(z)$ and $U(z)$ are the Brunt–Väisälä frequency and the background shear current and the value of $\Phi(z)$ is normalized by its maximal value. Then $\eta(x, t)$ is the isopycnal surface with maximum displacement.

Usually, for calculations of the coefficients of the K-dV equation only a single vertical profile of stratification is used assuming the density to be horizontally uniform. Analysis of Ivanov et al. (1992), made without shear flow for the deep water region of the Mediterranean, has shown that the variability of the parameters c and β is related mainly to variability in water depth, but the nonlinear parameter is very sensitive to variations of the vertical stratification. The shelf/slope zone is generally characterized by large bottom slope and large variations in stratification and shear flow and, using mean stratification, can be inaccurate in the calculation of α, β, and c. Variations in the coefficients of the K-dV equation along the wave ray in the coastal zone of the NWS are analyzed in section 4. The analysis shows strong spatial variability in all coefficients that influence the variability of the internal wave field. Account must be taken of the horizontal variability of the ocean medium, and accordingly the K-dV equation must be modified in the following way. If the horizontal vari-

Unauthenticated | Downloaded 09/25/22 05:48 AM UTC

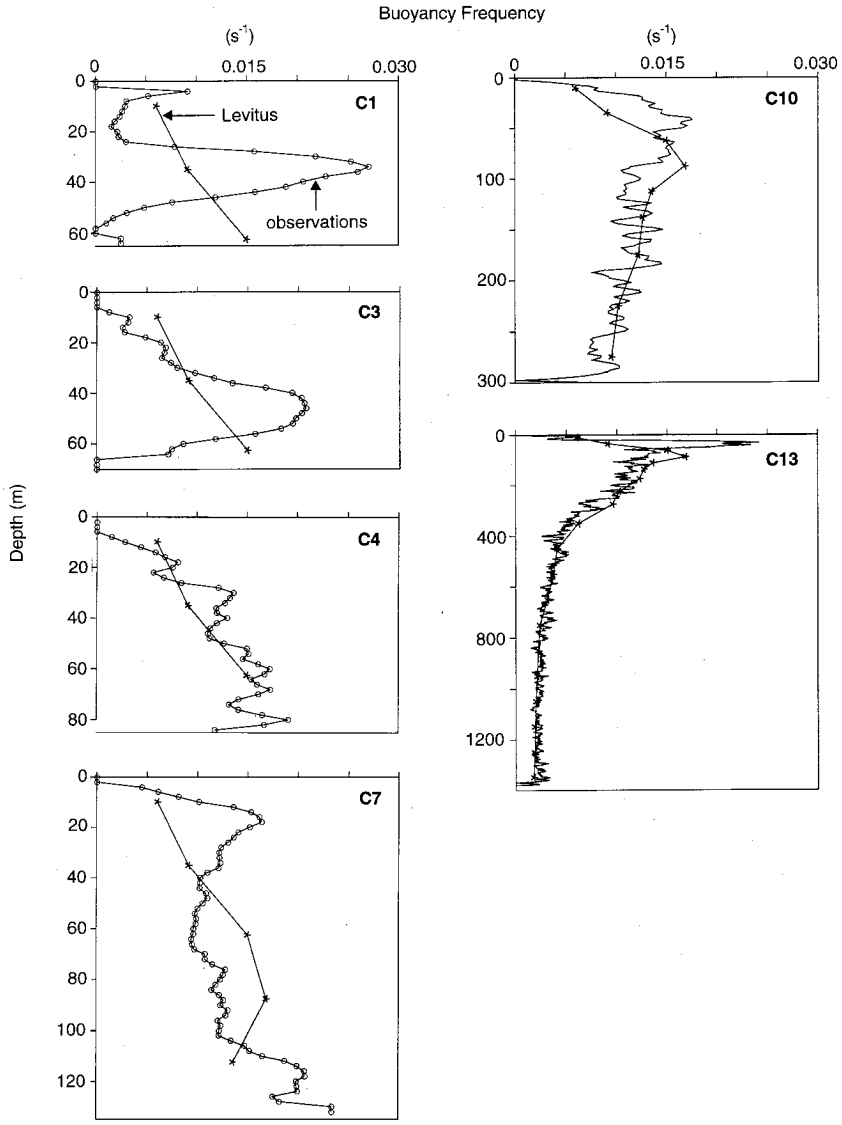

FIG. 4. Vertical profiles of the Brunt–Väisälä frequency calculated from CTD data of 1995 at locations C1, C3, C4, C7, C10, and C13 and calculated from Levitus climatic data.

ability is smooth, the reflection of the wave energy from the shelf can be ignored and a solution can be sought for the vertical displacement of the pycnocline in the form $\eta(t, x)\Phi(z, \epsilon x)$, where Φ is again the vertical structure of the pycnocline displacement, found from Eq. (4), and the small parameter ϵ characterizes the smoothness of the horizontal inhomogeneity of the ocean medium. Again using the asymptotic procedure (Pelinovsky et al. 1977; Zhou and Grimshaw 1989), the following equation [a generalized form of (1)] can be obtained:

$$\frac{\partial \eta}{\partial t} + c\frac{\partial \eta}{\partial x} + \alpha\eta\frac{\partial \eta}{\pi x} + \beta\frac{\partial^3 \eta}{\partial x^3} + \frac{c}{2Q}\frac{dQ}{dx}\eta = 0, \quad (5)$$

where

$$Q = \frac{c^2\int_{-H}^{0}(c - U)(d\Phi/dz)^2\,dz}{c_0^2\int_{-H}^{0}(c_0 - U_0)(d\Phi_0/dz)^2\,dz} \quad (6)$$

and values with index ''0'' are the values at any fixed point x_0 (it is convenient to use the origin and put $x_0 = 0$, usually corresponding to the deepest water station).

If nonlinearity and dispersion are ignored, Eq. (5) is immediately solved to give

$$\eta(x, t) = a(x)F\left(t - \int_0^x \frac{dl}{c(l)}\right), \quad (7)$$

where $a(x)$ is the variable wave amplitude

Unauthenticated | Downloaded 09/25/22 05:48 AM UTC

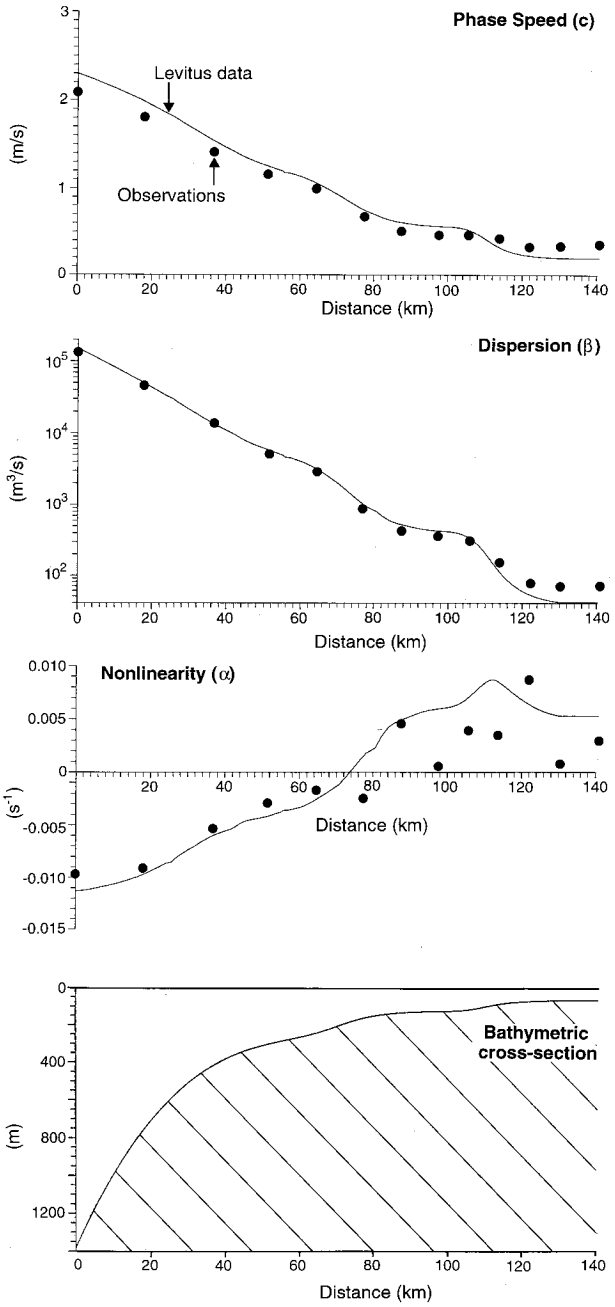

FIG. 5. Coefficients of the K-dV equation calculated from CTD data of 1995 (points) and from Levitus climatic data (solid line) as a function of distance across the shelf-break region. The bathymetric cross section is also shown.

$$a(x) = \frac{a_0}{\sqrt{Q(x)}} \tag{8}$$

and $F(t)$ is the arbitrary input form of the internal wave (generally, for deep water, F can be considered in the form $F = \sin\omega t$, where ω is the frequency of the internal tide) with initial amplitude a_0. The variation of the wave amplitude (the factor Q) is a result of slowly varying depth and of horizontal variability in background density and shear flow. This is discussed further in section 4.

The propagation of an internal wave in the coastal zone is accompanied by energy losses due to bottom friction and horizontal diffusion. The modified K-dV equation incorporating the linear effect of the weak molecular viscosity for the internal waves is discussed by Grimshaw (1983) and Smyth (1988). Consider two forms of damping of the internal wave: The first is related with boundary-layer viscosity, and the second to the viscosity of the fluid as a whole. The representations of dissipation in the modified K-dV equation have different characteristics: first, dissipation is described by the integral term, and second, dissipation is described by the differential term of second order. For laboratory conditions the first term is preferable, but the real boundary layer for the ocean is turbulent and its linear description is incorrect. Usually, the turbulent boundary layer is parameterized by the empirical expression for the bottom friction stress, for example, in the Chezy form (Gallagher and Munk 1971) or quadratic bottom friction:

$$\tau_b = \rho k u|u|, \tag{9}$$

where ρ is the seawater density, u is the near-bottom velocity outside of the boundary layer (or the depth-averaged velocity for barotropic flow), and k is an empirical coefficient representing the Chezy friction ($k \sim 0.001 - 0.0026$, see Voltsinger et al. 1989). The second form of the linear dissipation (horizontal viscosity) achieves smoothing of the short-length horizontal variations of the wave field, but the coefficient of the laminar viscosity ($\nu = 10^{-6}$ m^2 s^{-1}) is replaced by the empirical coefficient of the turbulent horizontal eddy viscosity, which can be larger than the laminar value by many orders of magnitude; for example, Liu et al. (1985) used $\nu = 10 - 30$ m^2 s^{-1} for soliton modeling in the Sula Sea; in a study of internal waves in the New York Bight, Liu (1988) estimated the horizontal eddy viscosity to be of the order of 1 m^2 s^{-1}; Sandstrom and Oakey (1995) obtained an average value of ν for the Scotian Shelf of 0.2 m^2 s^{-1}. Taking into account the empirical character of dissipative approximations, the corresponding equation can be written as (separate parts of the modified K-dV equation incorporating both dissipative approximations were obtained for surface and internal waves in papers by Klevanny and Pelinovsky 1978; Grimshaw 1983; Smyth 1988; Voltsinger et al. 1989; Zhou and Grimshaw 1989)

$$\frac{\partial\eta}{\partial t} + c\frac{\partial\eta}{\partial x} + \alpha\eta\frac{\partial\eta}{\partial x} + \beta\frac{\partial^3\eta}{\partial x^3} + \frac{c}{2Q}\frac{dQ}{dx}\eta + \frac{kc}{h^2}\eta|\eta| - \nu\frac{\partial^2\eta}{\partial x^2} = 0, \tag{10}$$

where h is the effective depth, representing the vertical scale of the mode of the internal wave, written as

$$h = \sqrt{\beta/c}. \tag{11}$$

Unauthenticated | Downloaded 09/25/22 05:48 AM UTC

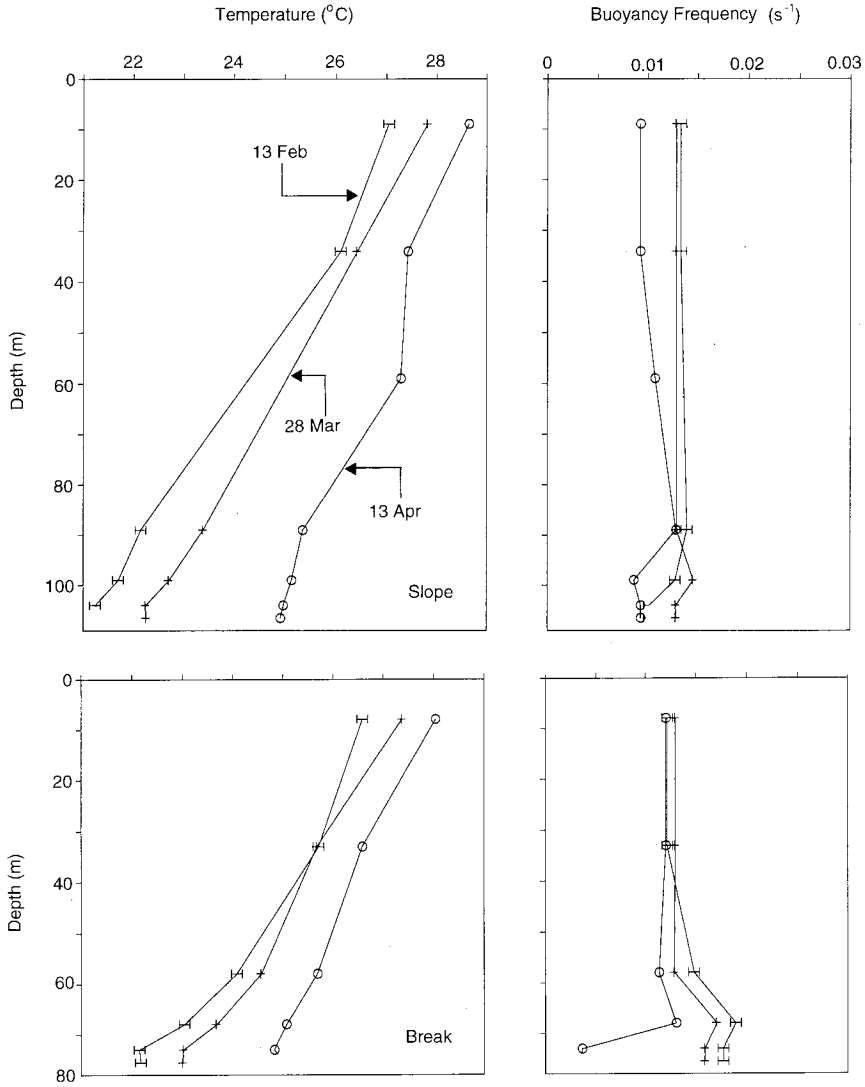

FIG. 6. Vertical profiles of temperature and Brunt–Väisälä frequency calculated as 4-day averages from data of 1992. Profiles are shown from three different times and for locations slope and break.

In the first approximation, the influence of the background shear flow on ''dissipative'' coefficients k and ν is neglected, considering them as constants in the numerical simulation of the internal tide transformation.

Equation (10), after substituting for s and ξ, where

$$s = \int_0^x \frac{dx}{c(x)} - t, \tag{12a}$$

and

$$\xi = \eta\sqrt{Q(x)} \tag{12b}$$

is reduced to

$$\frac{\partial\xi}{\partial x} + \frac{\alpha}{c^2\sqrt{Q}}\xi\frac{\partial\xi}{\partial s} + \frac{\beta}{c^4}\frac{\partial^3\xi}{\partial s^3} + \frac{kc}{\beta\sqrt{Q}}\xi|\xi| - \frac{\nu}{c^3}\frac{\partial^2\xi}{\partial s^2} = 0; \tag{13}$$

this equation is valid to first order in the wave amplitude ($a/H \ll 1$), for long waves ($H/\lambda \ll 1$) in a weak viscous fluid ($\nu/c\lambda \ll 1$ and $kac\lambda/\beta \ll 1$) with the smooth horizontal inhomogeneities of the ocean medium ($\lambda/L \ll 1$), where L is the characteristic horizontal scale of variations in depth, Brunt–Väisälä frequency, and background shear flow.

The generalized K-dV equation (13) is the basic model used for the internal tide transformation on the NWS. Physically, the boundary problem of the spatial transformation of the internal wave, which is periodical in time, is studied. Mathematically this is an initial value problem (Cauchy problem) for Eq. (13), where the evolution coordinate (''time'') is the spatial coordinate. It is necessary to solve (13) for the initial condition

$$\xi(s, x = 0) = a_0F(\omega, s) \tag{14}$$

Unauthenticated | Downloaded 09/25/22 05:48 AM UTC

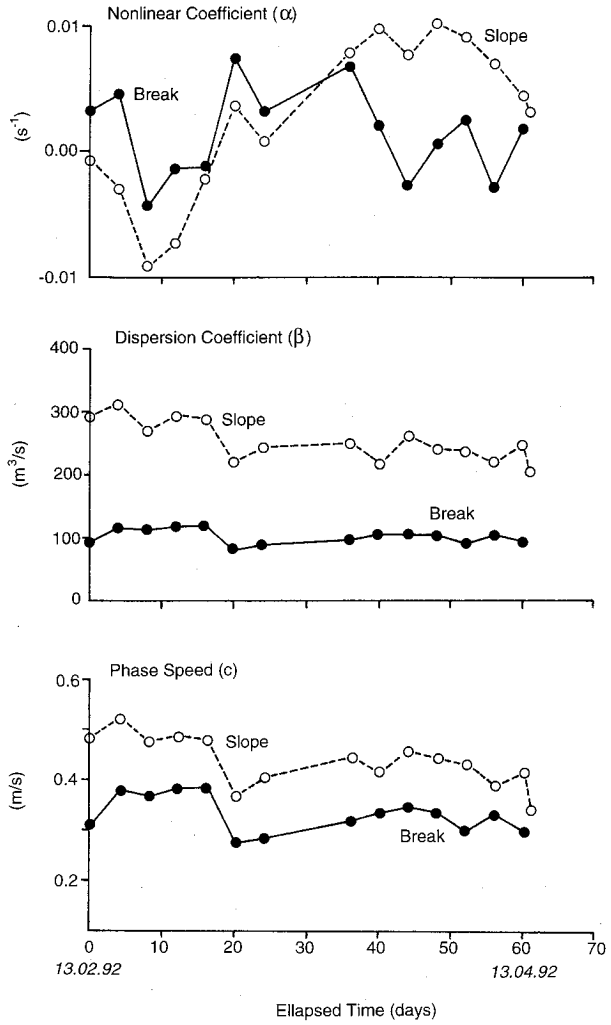

FIG. 7. Temporal variability over a 2-month period of coefficients of the K-dV equation calculated from 4-day average data from 1992 for the slope and break locations.

and periodic boundary conditions

$$\xi\left(s + \frac{2\pi}{\omega}, x\right) = \xi(s, x), \tag{15}$$

where a_0 and ω are the input amplitude and frequency of the applied internal tide having the periodic form $F(t)$. It is easy to show that the following integral relation is obtained from (13):

$$\frac{d}{dx}\int \xi(s, x)\, ds = -\frac{kc}{\beta\sqrt{Q}}\int \xi(s, x)\,|\xi(s, x)|\, ds, \tag{16}$$

where the integrals are over a wave period. This shows that the average level of the pycnocline is changed in space and is related only with the Chezy friction coefficient within the model. It is not the ''setup'' effect in the pure form because the real setup (or setdown) of the pycnocline surface depends on the product: $\eta(t, x) \times \Phi(z, x)$. The relation (16) is convenient to test the algorithms of the numerical solution of the generalized K-dV equation. In particular, when bottom friction is not taken into account ($k = 0$), from (16) we have the simple conservation law:

$$\int \xi(s, x)\, ds = \text{const.} \tag{17}$$

Similarly, from (13) after multiplying by ξ, the second integral relation is obtained;

TABLE 2. The nonlinear coefficient (α) for the slope and shelf locations calculated both with and without the influence of background shear flow.

Date 1992	No shear	Shear
	Slope	
10 Feb–20 Feb	0.438×10^{-3}	-0.227×10^{-3}
20 Feb–30 Feb	-3.316×10^{-3}	-3.524×10^{-3}
01 Mar–10 Mar	1.400×10^{-3}	0.913×10^{-3}
17 Mar–27 Mar	-1.322×10^{-3}	-1.677×10^{-3}
27 Mar–06 Apr	0.392×10^{-3}	0.285×10^{-3}
06 Apr–16 Apr	0.201×10^{-3}	0.294×10^{-3}
	Shelf	
10 Feb–20 Feb	4.721×10^{-3}	4.179×10^{-3}
20 Feb–1 Mar	-2.069×10^{-3}	-3.572×10^{-3}
01 Mar–10 Mar	3.659×10^{-3}	0.775×10^{-3}
17 Mar–27 Mar	1.333×10^{-3}	0.507×10^{-3}
27 Mar–06 Apr	-2.013×10^{-3}	-0.597×10^{-3}
06 Apr–16 Apr	-1.077×10^{-3}	-0.759×10^{-3}

TABLE 1. Averaged values of the phase speed (c) and coefficients of nonlinearity (α) and dispersion (β) and their rms deviations for stratification data from 1992.

Averaging period	$\bar{\alpha}$	$\Delta\alpha$	$\bar{\beta}$	$\Delta\beta$	$\bar{c}$	Δc
		Slope				
13 Feb–08 Mar	-2.56×10^{-3}	4.08×10^{-3}	273.7	30.4	0.46	0.050
20 Mar–13 Apr	7.35×10^{-3}	2.30×10^{-3}	234.0	17.4	0.42	0.034
13 Feb–13 Apr	2.73×10^{-3}	5.92×10^{-3}	252.5	31.4	0.44	0.047
		Break				
13 Feb–08 Mar	1.61×10^{-3}	3.80×10^{-3}	103.0	15.4	0.34	0.046
20 Mar–13 Apr	1.09×10^{-3}	3.11×10^{-3}	98.8	5.7	0.32	0.018
13 Feb–13 Apr	1.35×10^{-3}	3.48×10^{-3}	100.9	11.8	0.33	0.036

Unauthenticated | Downloaded 09/25/22 05:48 AM UTC

TABLE 3. The coefficients α, β, c, calculated as the average of the six 10-day values in Table 2, and their rms deviations calculated with and without the influence of background shear flow.

Location		$\bar{\alpha}$	$\Delta\alpha$	$\bar{\beta}$	$\Delta\beta$	$\bar{c}$	Δc
Slope	No shear	-3.70×10^{-4}	1.54×10^{-3}	260.77	18.61	0.43	0.031
Slope	Shear	3.71×10^{-4}	3.21×10^{-3}	217.71	23.09	0.43	0.054
Shelf	No shear	7.59×10^{-4}	2.69×10^{-3}	93.34	9.61	0.30	0.029
Shelf	Shear	-3.26×10^{-4}	3.42×10^{-3}	72.47	10.55	0.30	0.051

$$\frac{d}{dx}\int \xi^2(s, x)\, ds = -\frac{2kc}{\beta\sqrt{Q}}\int \xi^2|\xi|\, ds - \frac{2\nu}{c^3}\int\left(\frac{\partial\xi}{\partial s}\right)^2 ds, \tag{18}$$

and when dissipative effects are not taken into account, the second conservation law is obtained, which shows the conservation of the energy flux through the vertical cross section

$$\int \xi^2(s, x)\, ds = \text{const.} \tag{19}$$

In comparison to the K-dV equation with constant coefficients, where there are an infinite number of conservation laws, the variable-coefficient K-dV equation (generalized K-dV equation without dissipative terms) has only two conserved quantities. The K-dV equation with constant coefficients is a fully integrable system and has an exact solution for any initial conditions, while the variable-coefficient K-dV equation or the generalized K-dV equation (13) do not have such properties and numerical methods must be used. Such solutions will be described in section 5.

4. Variability in the coefficients of the K-dV equation

In studying the transformation of the internal tide on the NWS it is necessary at first to investigate the spatial and temporal variability of the coefficients of the K-dV equation (1) based on observations.

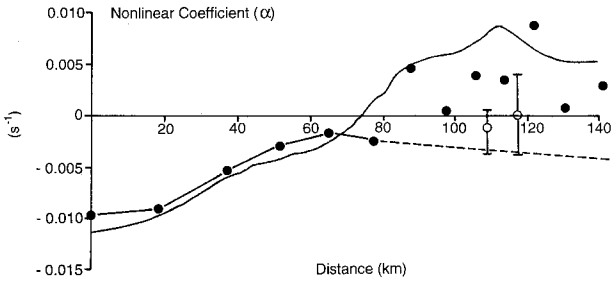

FIG. 8. Cross-shelf distribution of the nonlinear coefficient (α) calculated from Levitus climatic data (solid line) and from 1995 data without shear flow (solid line with points). Vertical lines show the variability at the slope and break calculated with shear flow and showing mean, maximum, and minimum values. The dashed line defines a lower boundary of α.

a. Stratification from 1995 observations

In this section, observations are used from a CTD survey carried out on the NWS in January 1995 (summer). At each of 13 locations, ranging in depth from 65 to 1382 m (Fig. 1), a sequence of repeated profiles were measured every 30, 60, or 90 min, depending on the water depth, over a 13-h cycle. These profiles have been averaged at each location to remove variability induced from internal waves, and the resulting CTD cross section is used to define the coefficients α, β, and c.

Vertical profiles of the Brunt–Väisälä frequency, calculated from the CTD measurements of 1995, are shown in Fig. 4 for 6 of the locations at different water depths between 65 and 1382 m. For comparison, buoyancy frequency profiles from climatic data are calculated from profiles of the temperature and the salinity for this region in a summer–autumn period taken from the atlas of Levitus (1982). This provides a single profile for deep water that is truncated at the appropriate depth in shallower water. For depths greater than 200 m there is close agreement between the measured and climatic profiles except for differences in the depth of the maximum value of Brunt–Väisälä frequency. For shallow water the observed profiles differ from the Levitus values; in particular, the pycnocline is narrower than the climatic pycnocline. This can be expected due to bottom boundary layer mixing over the shelf.

Initially, all coefficients of Eq. (1) are calculated without the effects of background shear flow. The phase speed and coefficients of dispersion and nonlinearity are calculated from (2), (3), and (4) with $U = 0$. The results from the climatic profile (Levitus data) of buoyancy frequency and from observations are plotted in Fig. 5 as a function of distance across the slope/shelf region. It is seen that the estimates of phase speed and the dispersion coefficient from climatic data and those from the observations are very similar for all water depths. Therefore, the climatic estimates of these parameters can be used as a first approximation for the prediction of the kinematic characteristics of the internal wave field for this region. The same conclusions were obtained for the Mediterranean Sea (Ivanov et al. 1992). Both c and β depend primarily on the depth with a weaker dependance on the shape of the vertical profiles of buoyancy frequency.

Both c and β can be expressed as functions of the depth by regressions:

Unauthenticated | Downloaded 09/25/22 05:48 AM UTC

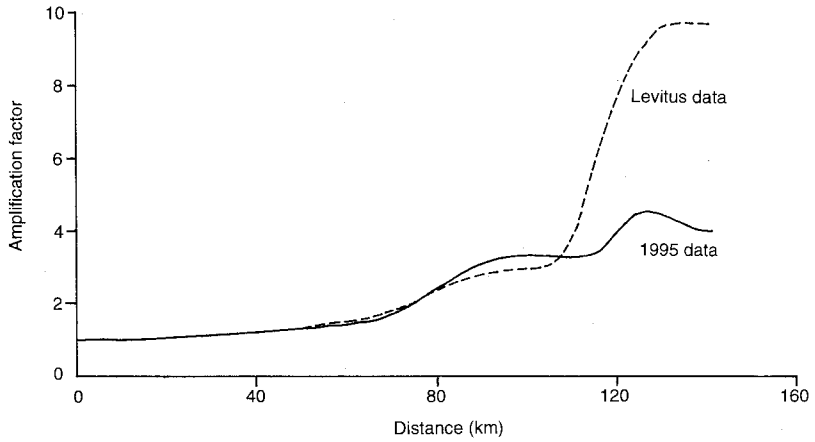

FIG. 9. Cross-shelf amplitude amplification calculated from linear theory of long internal waves for data from 1995 (solid line) and Levitus climatic data (dashed line).

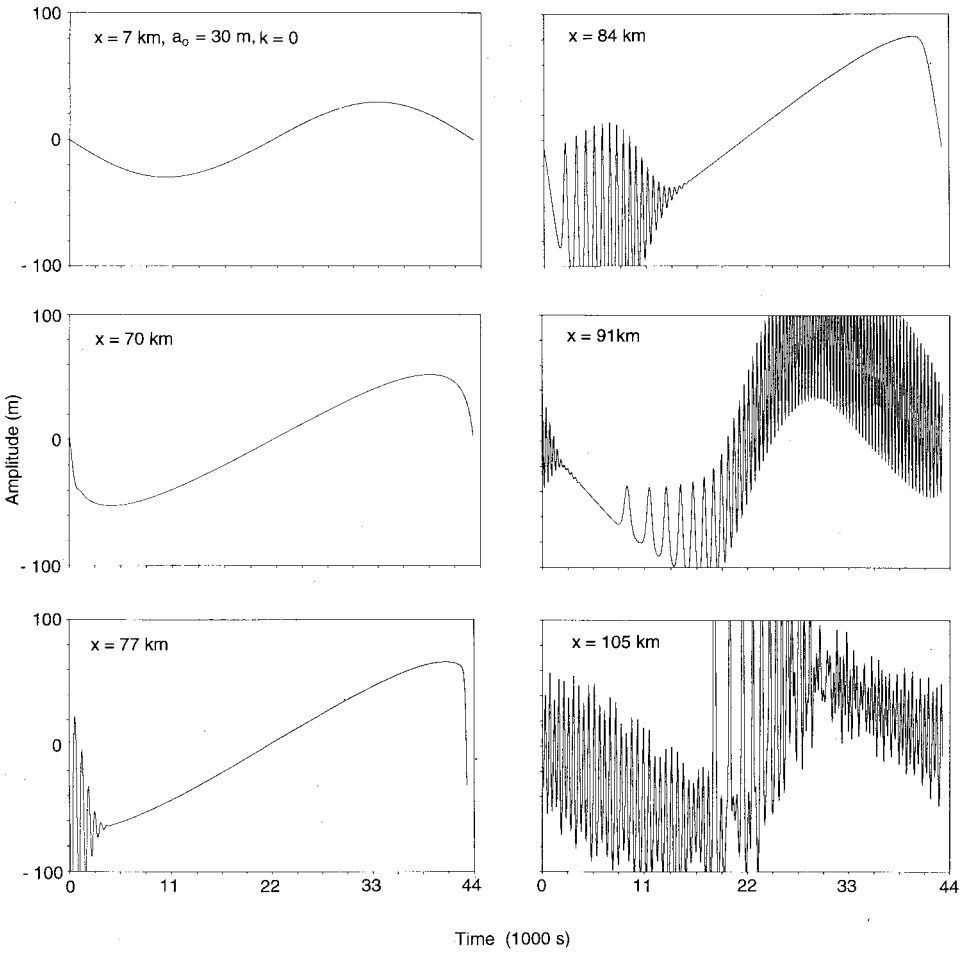

FIG. 10. Numerical results from the generalized K-dV equation. The waveform over one period is shown at different distances (x) from the origin. Calculations are for data from 1995. Initial amplitude 30 m, $k = 0$.

Unauthenticated | Downloaded 09/25/22 05:48 AM UTC

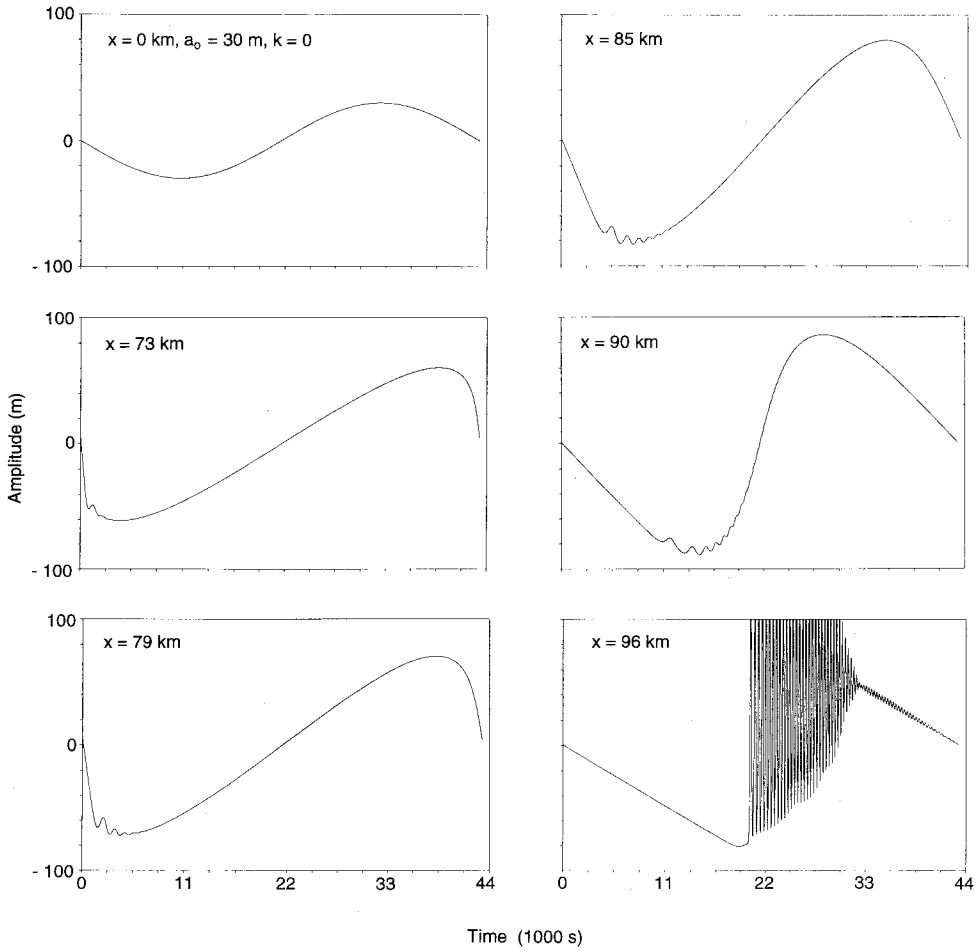

FIG. 11. As in Fig. 10 but for the Levitus climatic data. Initial amplitude 30 m, $k = 0$.

$$c = 0.021H^{0.67} \tag{20}$$

$$\beta = 0.00145H^{2.6}. \tag{21}$$

The power coefficients in (20) and (21) are relatively close to the theoretical values (1 and 3, respectively) for an exponential stratification of the density field, which can be used for rough estimates of the phase speed and the dispersion parameter for long waves.

The nonlinearity coefficient, which is sensitive to the shape of the buoyancy frequency profile, has a more complex behavior than β and c. This sensitivity can be understood by considering the simple case of a two-layer density stratified ocean (two uniform layers of depth h_1 and h_2 separated by density jump $\Delta\rho$). For this model the nonlinear coefficient is

$$\alpha = 3c(h_1 - h_2)/2h_1h_2. \tag{22}$$

It is clear that if the pycnocline is close to the sea surface, that $\alpha < 0$. In shallow water, if the pycnocline is close to the sea bottom, $\alpha > 0$. In the case of the NWS, the pycnocline is close to the sea surface in deep water, and it is close to the sea bottom in shallow water (Fig. 4). Mathematically the sign of nonlinear coefficient depends on the magnitude of $\int(d\Phi/dz)^3\,dz$ on both sides of the pycnocline [see (2)]. Large and asymmetric gradients of the eigenmode influence the sign of the nonlinear coefficient. Therefore, α depends on the details of the vertical structure of the Brunt–Väisälä frequency.

There is close agreement between α calculated from the climatic profile and the observations of the Brunt–Väisälä frequency for the deep water only (between locations C13 and C9), where the profile differences are less than for the shallow water. The sign of α is negative for the deep water, as found with calculations for many regions of the World Ocean (Ostrovsky and Stepanyants 1989). In this deeper region of the NWS, α can be approximated by the regression

$$\alpha = -3 \times 10^{-5}H^{0.82}. \tag{23}$$

From approximately 300-m depth and shallower, a region of strong variability of the nonlinear coefficient begins. Data from Levitus (1982) suggests α changes sign near a depth of 180 m, being positive at shallower depths (this was not mentioned in the theoretical interpretation of the internal tide transformation on the NWS in the paper by Smyth and Holloway 1988). From

Unauthenticated | Downloaded 09/25/22 05:48 AM UTC

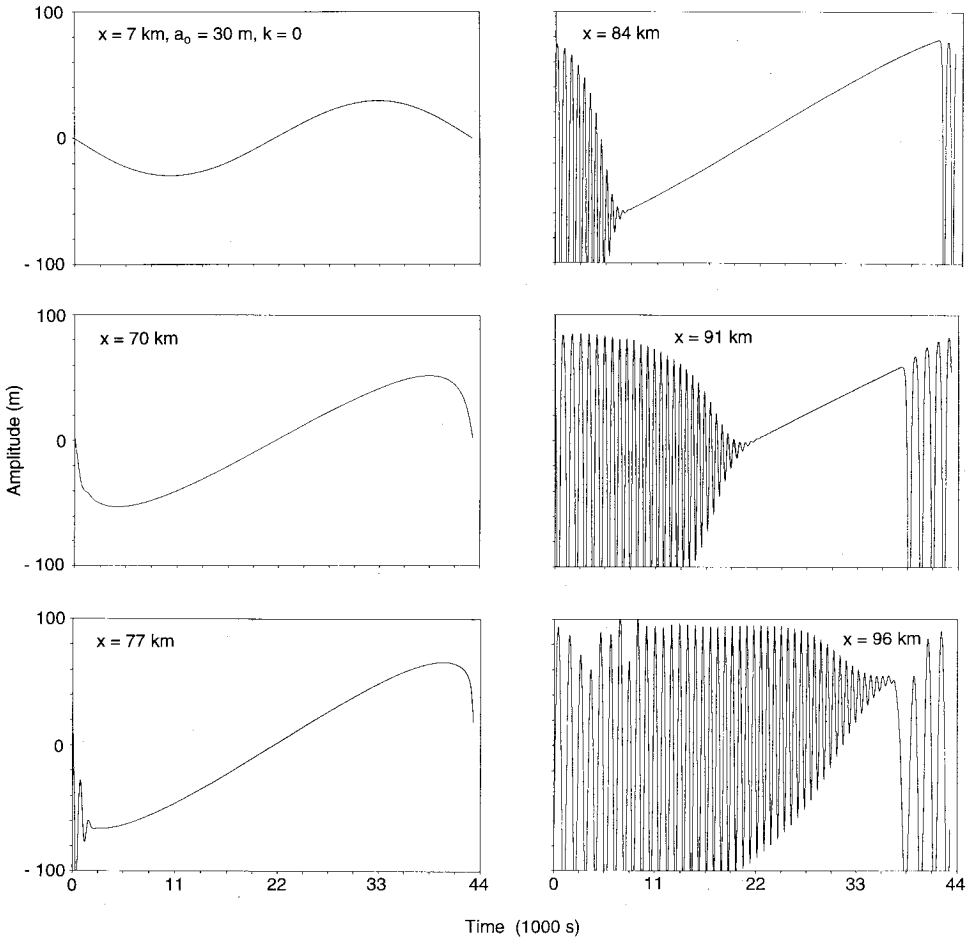

FIG. 12. As in Fig. 10 but for the nonlinear coefficient approximated by the dashed line in Fig. 8. Initial amplitude 30 m, $k = 0$.

observations in 1995 α is positive for depths smaller than 150 m with large variations in magnitude. The change in sign of α within the model of the K-dV equation was predicted in the nonlinear theory of internal waves long ago, but here direct confirmation of such behavior in α is observed. This change in sign of α is very important in the K-dV equation as it leads to interesting features in the theoretical analysis of the dynamics of internal solitons and cnoidal waves (Pelinovsky and Shavratsky 1976, 1977; Djordjevic and Redekopp 1978; Knickerbocker and Newell 1980; Helfrich et al. 1984; Malomed and Shrira 1991) and can have significant influence on the transformation of the internal tide.

Before performing numerical simulations of internal wave transformation, it is necessary to understand how often this change in the sign of α can occur. The NWS is characterized by strong internal tides with large amplitudes in comparison with other regions of the Indian Ocean (Morozov 1995). Such intensive internal tides influence the temperature and salinity profiles in the shelf zone and lead to large (compared to the water depth) vertical excursions of the pycnocline. This fact is important in determining the sign of α because, without shear flow, the location of the buoyancy frequency peak near the sea surface or near the sea bottom defines the sign of α as negative or positive, respectively. The temporal variability of α in the shelf zone of the NWS will be studied in section 4b.

b. Effects of stratification on α, β, and c

For the study of temporal variability of the coefficients of the K-dV equation, time series records are used of the stratification and velocity fields obtained in 1992 from the locations *Slope*, *Break*, and *Shelf* (see Fig. 2). The shape of the temperature and buoyancy frequency profiles are shown in Fig. 6 for *Slope* and *Break* for selected times between 13 February and 13 April 1992. The values are calculated from 4-day averages of the temperatures. For both slope and break, there are significant changes in the temperature profiles between the different times although the changes in the Brunt–Väisälä frequency are relatively small with the largest

Unauthenticated | Downloaded 09/25/22 05:48 AM UTC

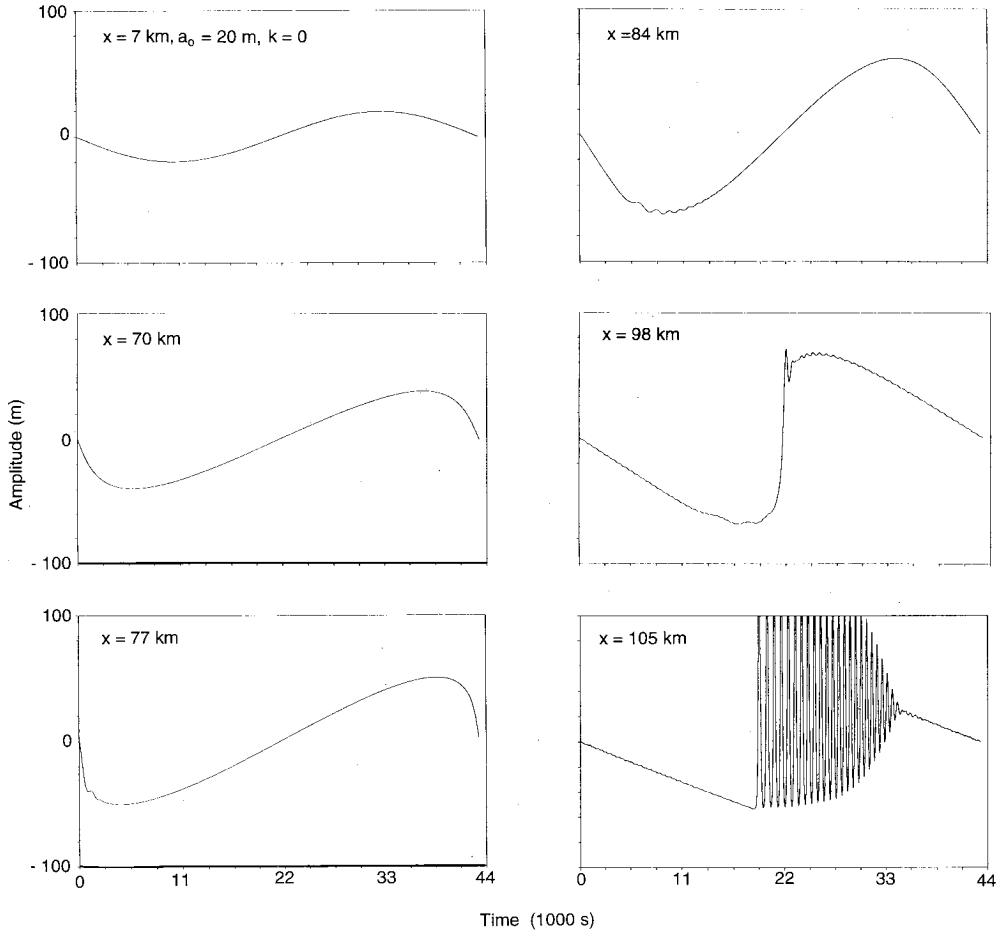

FIG. 13. As in Fig. 10 but for data from 1995. Initial amplitude 20 m, $k = 0$.

changes occurring near the seabed. However, the variations in vertical profiles of the buoyancy frequency are enough to cause large variations in the coefficients of the K-dV equation, where the nonlinear coefficient is sensitive to variations of the vertical density stratification.

The temporal variation of the coefficients of the K-dV equation, calculated without background shear flow, for the period 13 February–13 April 1992 are shown in Fig. 7 for slope and break locations. As expected, there is a large variation in the nonlinear coefficient for both locations, from negative values to positive values, while there are only small deviations for the dispersion coefficient and the phase speed. Because the buoyancy frequency profiles for the two locations vary with season, it is interesting to compare the mean values from February to April and their deviations (rms values). These values are given in Table 1. It can be seen that at the slope where the depth is more than 100 m, the sign of the mean value of α is negative for summer (February) and positive for autumn months (March–April). For the break where the internal waves have broken and the pycnocline is located near the bottom for all months of observation, the mean value of α is positive, but instantaneous values may be negative. The deviations of the nonlinear coefficient can be over double the averaged value, underlining the strong variability of this coefficient. The coefficients β and c are more stable, their mean values being similar from one month to the next and the deviations smaller compared to the averaged values.

c. *Influence of the background shear flow on α, β, and c*

The influence of shear flow on the coefficients of the K-dV equation is studied on the basis of observations from two locations: slope and shelf for the period 10 February to 16 April 1992. Six 10-day averages of temperature and velocity are used for calculation of the Brunt–Väisälä frequency profile, the onshore-velocity shear profile, and the subsequent coefficients of the K-dV equation. The nonlinear coefficients are calculated both with and without shear flow and are given in Table 2. It is seen that the background flow generally changes the magnitude of the nonlinear coefficient by up to one

Unauthenticated | Downloaded 09/25/22 05:48 AM UTC

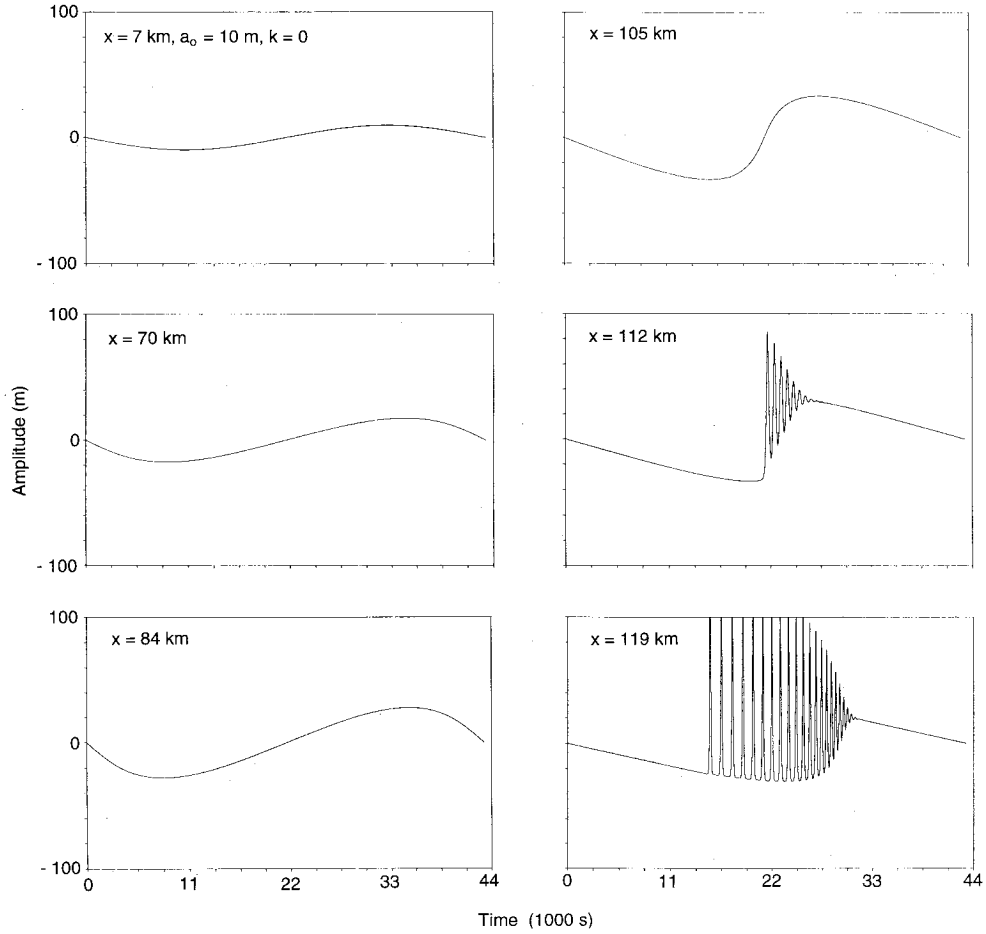

FIG. 14. As in Fig. 10 but for data from 1995. Initial amplitude 10 m, $k = 0$.

order of magnitude and on one occasion changes the sign. Even larger changes in α would be expected if shorter averaging times were used to calculate the background conditions.

The influence of background flow is less on c and β. In particular, the phase speed does not change significantly (Table 3), only the rms value of its deviation is increased, but the relative error is small (less than 15%). The dispersion coefficient is decreased by approximately 20% when the background shear flow is taken into account (Table 3), but its rms deviation is increased.

The analysis shows that the phase speed and dispersion coefficient, with an accuracy of 15%–30%, is not strongly dependent on the background shear flow for the conditions of the NWS and reasonable estimates can be made of c and β based on climatic vertical structures of the temperature and salinity. The nonlinear coefficient for depths of 100 m and less is highly variable due to the background flow and the variations in the density stratification; $|\alpha|$ can be estimated as the order of 10^{-3} s^{-1}, and changes from positive to negative with no preferable value. The 10-day mean and maximum and minimum values of α from the slope and break are plotted in Fig. 8. Taking into account the large variability of α, the climatic function can be considered as an upper bound, and a lower bound can be taken from the minimum values, as shown in Fig. 8. These upper and lower bounds, along with the data of 1995, are used in the numerical simulation of the internal tide transformation.

d. Amplification factor

Taking into account the horizontal variability of the ocean, the variable-coefficient K-dV equation (5) [or (10)] is to be used for the calculation of the evolution of the internal tide on the NWS. This equation includes the factor Q that, in linear theory of long waves, describes the amplification of the wave amplitude when the initial wave propagates into shallow water. From (8), P can be defined as

$$P(x) = Q(x)^{1/2} \tag{24}$$

Unauthenticated | Downloaded 09/25/22 05:48 AM UTC

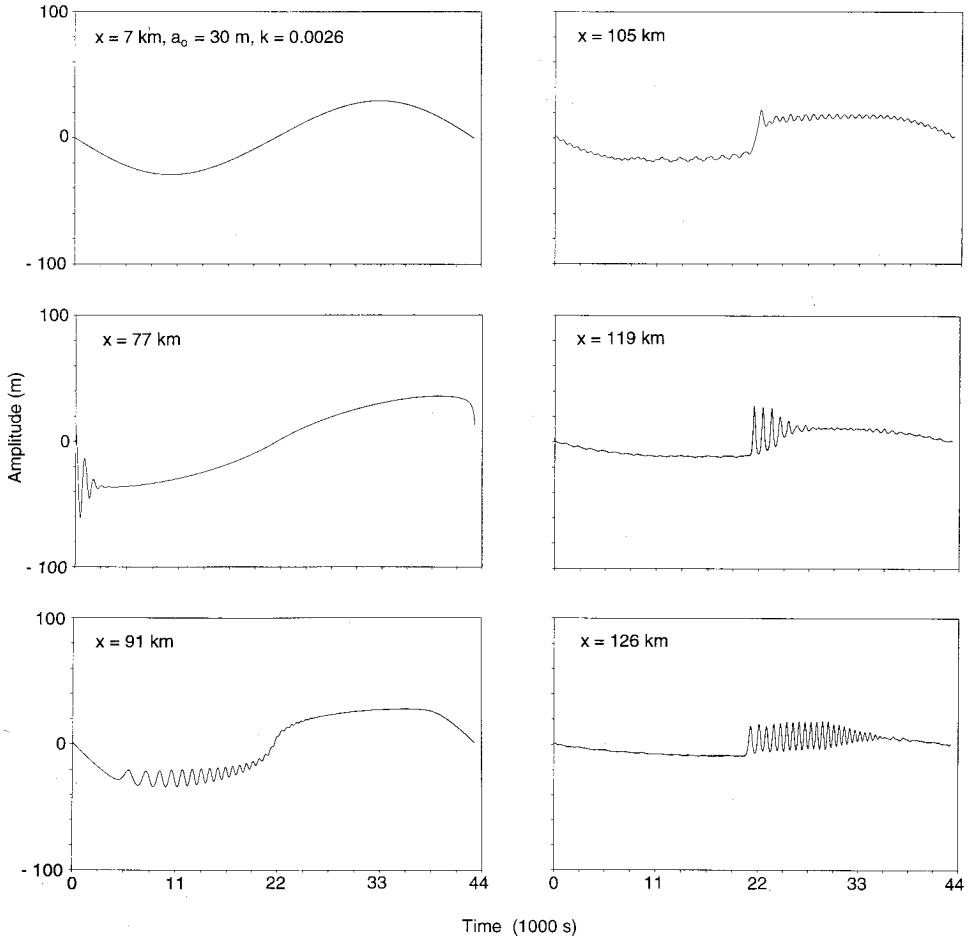

FIG. 15. As in Fig. 10 but for data from 1995. Initial amplitude 30 m, $k = 0.0026$.

and is the amplification factor from linear theory of long internal waves [where $P(0) = 1$]. This function, calculated from (6), is shown in Fig. 9 for both the ''climatic'' and observed ocean stratification. It is seen that the amplification is sensitive to the density stratification for depths less than 100 m and, in particular, its maximum is 10 based on climatic data and 5 based on observed data of 1995. Therefore, the estimates of the variation of wave amplitude with linear theory of long waves can easily be in error for shallow water regions. Similar estimates were carried out for the slope and break locations. The relative amplification factor ($P_{\text{break}}/P_{\text{slope}}$) is equal to 1.9 for climatic data and 1.1 for the 1995 observations. Similar estimates for the data from 1992 show that, with shear, the relative amplification factor is 1.2 and without shear is 1.4.

5. Finite difference scheme for the K-dV equation

The generalized K-dV equation (13) is solved numerically after writing it in a finite difference form:

$$\frac{\xi_j^{n+1} - \xi_j^{n-1}}{D} + \frac{\alpha_j}{c_j^2\sqrt{Q_j}}\xi_j^n\frac{\xi_{j+1}^n - \xi_{j-1}^n}{T} + \frac{\beta_j}{c_j^4}\frac{\xi_{j+2}^n - 2\xi_j^n + 2\xi_{j-1}^n - \xi_{j-2}^n}{T^3} + \frac{2kc_j}{\beta_j\sqrt{Q_j}}\xi_j^n|\xi_j^n| - \frac{2\nu}{c_j^3}\frac{\xi_{j+1}^n - 2\xi_j^n + \xi_{j-1}^n}{T^2} = 0. \quad (25)$$

For the first step the temporal difference $(\xi_j^{n+1} - \xi_j^{n-1})/2D$ is replaced by $(\xi_j^1 - \xi_j^0)/D$, where ξ_j^0 is the value of the initial wave form. This numerical scheme generalizes that developed for the K-dV equation by Berezin (1987) and for the variable-coefficients K-dV equation by Pelinovsky et al. (1994). The numerical stability criterion for (25) without the dissipative terms requires T and D to satisfy

$$\frac{D}{T}\left(\alpha\xi + \frac{3\sqrt{3}\beta}{2T^2}\right) < 1, \quad (26)$$

where the variability of quantities α, β, and ξ in the process of the wave evolution must be taken into ac-

Unauthenticated | Downloaded 09/25/22 05:48 AM UTC

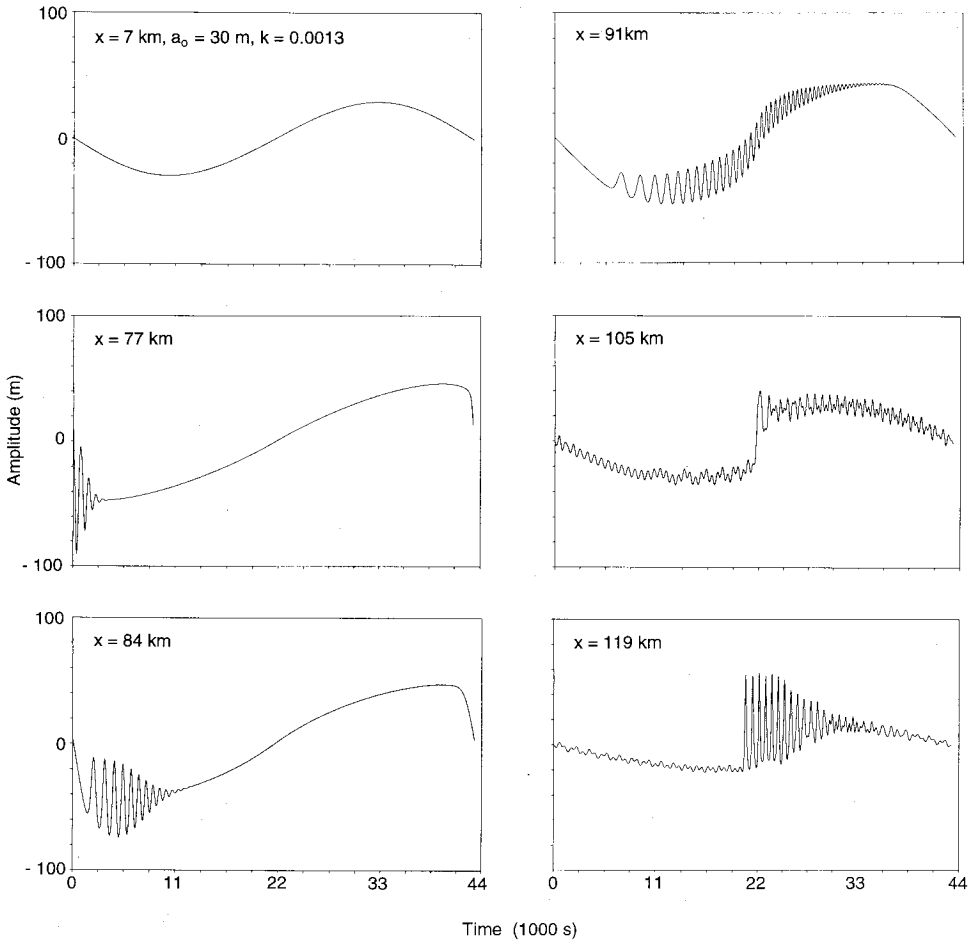

FIG. 16. As in Fig. 10 but for data from 1995. Initial amplitude 30 m, $k = 0.0013$.

count. For small values of T this condition can be simplified to

$$D < 0.38T^3/\beta. \tag{27}$$

In addition, T must be chosen so as to properly resolve the highest frequency waves that are generated by the model.

6. Numerical simulation of internal tide transformation

The model is used for the study of several scenarios of the transformation of the internal tide on the NWS. The first series of numerical experiments corresponds to the evolution of the internal wave starting at 1382-m depth, the farthest offshore location of stratification data. In all runs the initial wave period is 12 h with a sinusoidal form but with various amplitudes. The influence of nonlinear and dispersive effects on the internal tide propagation is studied for different approximations of hydrological data. It is important to note that the coordinate s is

$$s = \int_0^x \frac{dl}{c(l)} - t = \tau(x) - t, \tag{28}$$

where τ corresponds to the running time from $x = 0$ and s represents the time in the system where the coordinates are moving with the phase speed of a long wave. Results are shown as functions of time, neglecting the time taken for the signal to propagate across the model domain and at different values of x.

a. Results without dissipation

Figure 10 shows the wave form, computed without frictional dissipation ($k = 0$), at different distances from the origin, where the initial wave amplitude (a_0) is 30 m, using coefficients calculated from data of January 1995. The internal tide steepens and a shock is formed on the trailing edge of the wave (''back face'') at a distance of approximately 70 km (200-m depth). After further propagation undulations develop and the shock transforms to a group of solitary waves of depression (solitons). Such a process is well known for the internal tide transformation on the shelf for many regions of the

Unauthenticated | Downloaded 09/25/22 05:48 AM UTC

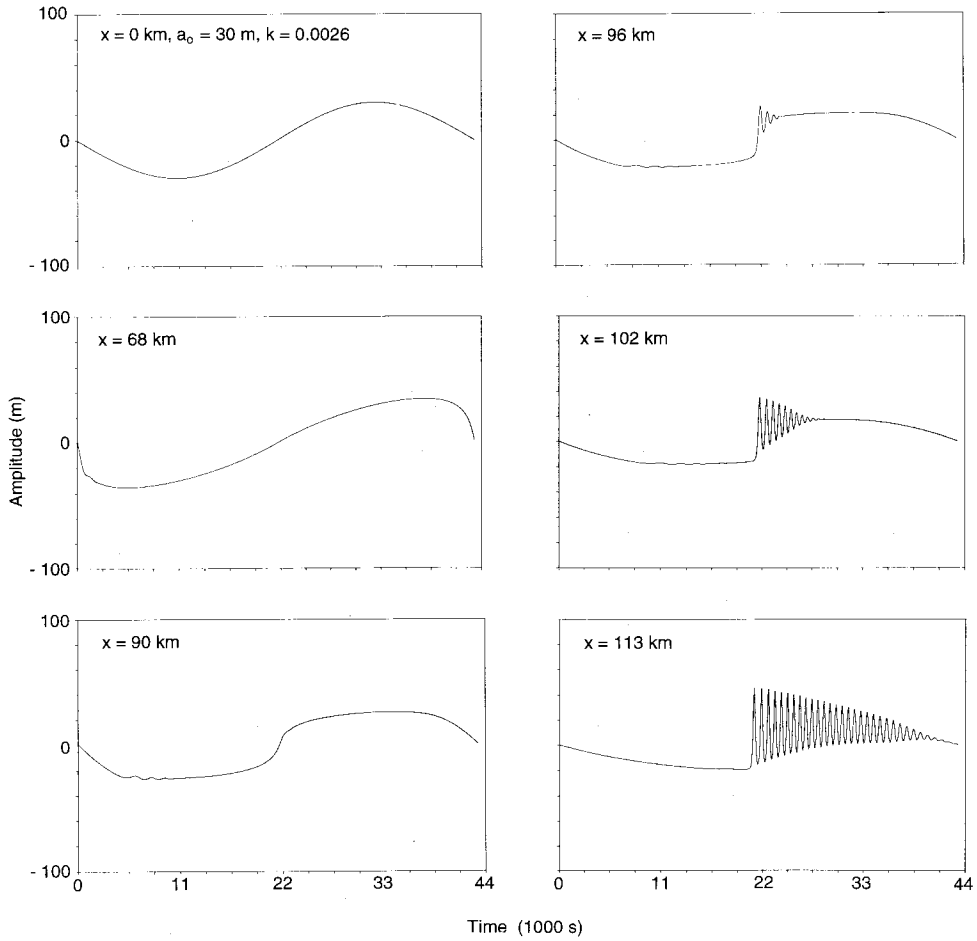

FIG. 17. As in Fig. 10 but for Levitus climatic data. Initial amplitude 30 m, $k = 0.0026$.

World Ocean (Halpern 1971; Holloway 1984, 1987; Goryachkin et al. 1992; Gan and Ingram 1992) and has been explained within the K-dV equation with constant coefficients (Lee and Beardsley 1974; Smyth and Holloway 1988; Goryachkin et al. 1992). On the NWS, the nonlinear coefficient has a change in sign at a depth of approximately 170 m, or a distance of 80 km. As a result, the previously generated negative solitons (waves of depression) cannot exist at such a change in sign of α, and the soliton group transforms to a dispersive wave train (see wave forms at distance 84 and 91 km in Fig. 10). In the shallower water α is positive and a shock begins to form on the ''front face'' of the internal tide and then to transform to a new ''positive'' soliton group (waves of elevation). As a result, there is a complex picture of soliton undulations along the internal tide (see the wave form at distance 105 km). In this case the transformation of the internal tide at the point of change in sign of α is the source of the variability of the short-period internal wave field and its randomization.

As pointed out in section 4, α is very sensitive to variations in stratification and shear flow. A simulation was carried out using the upper and lower bound curves of $\alpha(x)$ in Fig. 8. Results for the upper curve, representing the ''climatic'' coefficients from the Levitus data, are shown in Fig. 11. In this case, α changes sign at 75 km, farther offshore than for the measurements of 1995. As a result, the process of soliton formation on the back face (at the negative sign of α) is not completed and the internal tide is a smooth waveform up to a distance of 85 km. Farther inshore, the positive sign of α causes a shock to form on the forward face and a soliton group appears. This group is more regular than in Fig. 10 and occupies a narrower region of the waveform. The results obtained for the lower curve of $\alpha(x)$ in Fig. 8 where α is always negative are shown in Fig. 12. It is seen that the initial long wave transforms into a large number of short-period waves after a distance of approximately 90 km. In comparison with Figs. 10 and 11, where α passes through zero and nonlinearity ceases for a short time, the nonlinearity acts continuously and results in strong generation of solitons (Fig. 12). Hence, the waveform is seen to be sensitive to the variability of α, which in turn depends on the stratification and background shear flow.

The following series of numerical experiments illus-

Unauthenticated | Downloaded 09/25/22 05:48 AM UTC

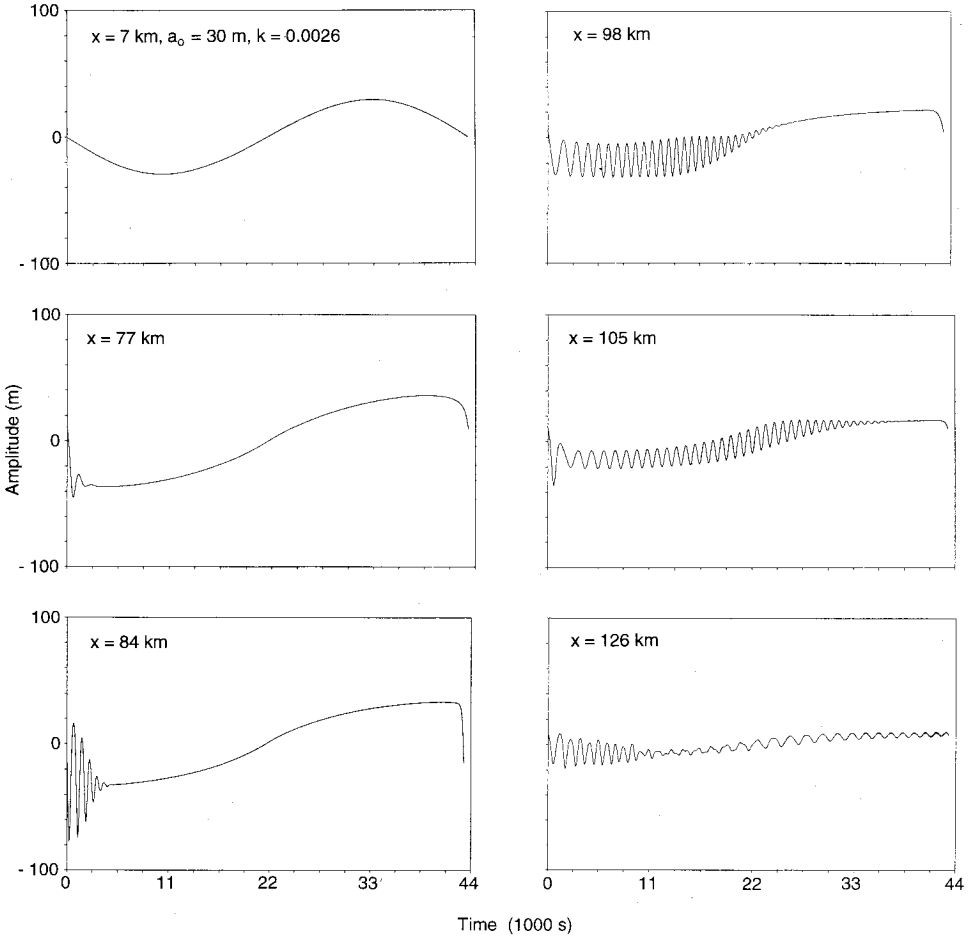

FIG. 18. As in Fig. 10 but for the nonlinear coefficient approximated by the dashed line in Fig. 8. Initial amplitude 30 m, $k = 0.0026$.

trates the influence of the initial wave amplitude on the process of the nonlinear wave transformation where coefficients are defined from the data of 1995. Waveforms are shown in Fig. 13 for an initial amplitude of 20 m. In this case the shock at the back face, at a distance of 80 km, does not contain solitons (compared with Fig. 10) and can be explained by the slower manifestation of the nonlinear effects resulting from the smaller initial wave amplitude. At greater distances the shock forms on the front face and a soliton group appears. This group is formed after 105 km compared to 90 km for an initial wave amplitude of 30 m. If the initial wave amplitude is 10 m, the nonlinear effects are even weaker (Fig. 14) and the shock on the back face does not appear. The forward shock forms after approximately 100 km and then transforms into a group of solitons. If the initial wave amplitude is 3 m, nonlinear effects are not visible and the internal tide does not change from its sinusoidal form.

It is interesting to analyze the variation of the amplitude of the internal tide during its transformation. If the initial amplitude is small and no solitons form, the amplification factor from linear theory of long internal waves (P), illustrated in Fig. 9, describes the amplification of the initial wave in agreement with the K-dV model (approximately three times over a distance of 100 km); see, for example, Figs. 13 and 14. However, soliton generation changes the picture of the smooth variation of the wave amplitude with distance and results in an approximate doubling of the amplitude of the short-period internal waves (Figs. 10 and 11). Calculated wave amplitudes can become more than the water depth in the coastal zone. To prevent this it is necessary to include dissipative effects in the K-dV model that are significant for shallow regions.

The numerical simulations discussed above, which exclude dissipative terms, show the generation of groups of short-period internal waves of solitonlike form and demonstrate the possibility of the appearance of the nonregular variability of the solitary wavefield due to changes in the sign of the nonlinear parameter. These calculations also show the sensivity of the wave transformation to the variability of the stratification and background flow, which influence the sign and magnitude

Unauthenticated | Downloaded 09/25/22 05:48 AM UTC

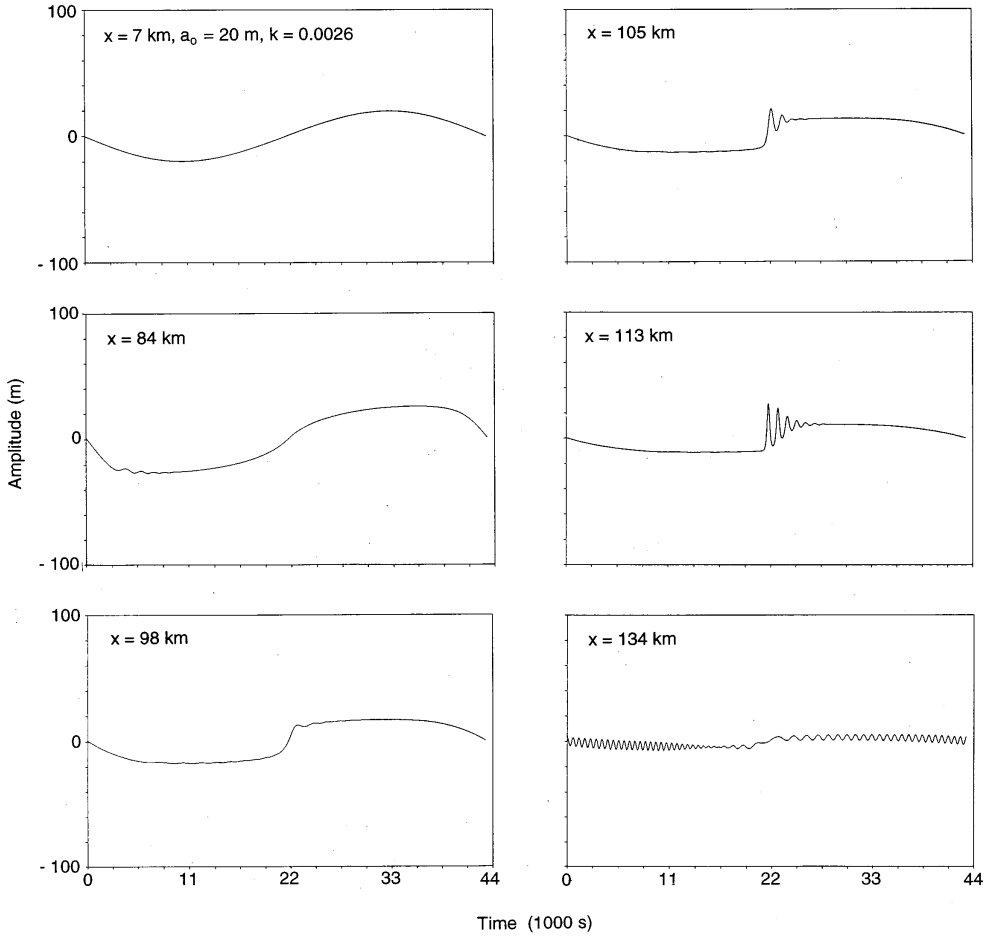

FIG. 19. As in Fig. 10 but for data from 1995. Initial amplitude 20 m, $k = 0.0026$.

of α. The nonlinear coefficient is critical for determining the waveform and results in complex behavior of the short-period internal waves in the coastal zone.

b. Effects of dissipation

Experiments including dissipative effects from horizontal diffusion and bottom friction are discussed. Both forms of dissipative mechanisms result in the same law of soliton damping (Grimshaw 1983; Miles 1983) and, as a result, can be modeled by only one mechanism. For example, horizontal eddy viscosity of 0.2–30 $m^2\ s^{-1}$ can provide observed damping of the solitary wave (Liu et al. 1985; Liu 1988; Sandstrom and Oakey 1995). But the effect on the long internal tide will be different: horizontal eddy viscosity smooths the large horizontal gradients, and quadratic bottom friction leads to damping of large amplitude waves. The numerical simulation of the K-dV equation results in a large amplitude internal tide in shallow water; hence modeling the influence of bottom friction is included. The calculations show that the turbulent horizontal diffusion with a coefficient $\nu = 2 \times 10^{-4}\ m^2\ s^{-1}$ has little effect on the process of nonlinear wave transformation for initial amplitudes up to 30 m (results are similar to Figs. 10–14). Figure 15 illustrates results of calculations with an initial amplitude of 30 m for a bottom friction coefficient $k = 0.0026$. Bottom friction significantly dampens the short-period waves and the soliton group is not as strong as results without friction (Fig. 10). At the same time the

TABLE 4. The averaged values of coefficients of the K-dV equation for 12-h data segments on 13 April 1992. Two different averaging periods are considered.

Location	α	β	c	α	β	c
Slope	3.44×10^{-3}	199	0.49	—	—	—
Break	1.61×10^{-3}	79.7	0.4	1.61×10^{-3}	79.7	0.4
Shelf	-0.77×10^{-3}	43.8	0.38	-0.18×10^{-3}	53.6	0.37

Unauthenticated | Downloaded 09/25/22 05:48 AM UTC

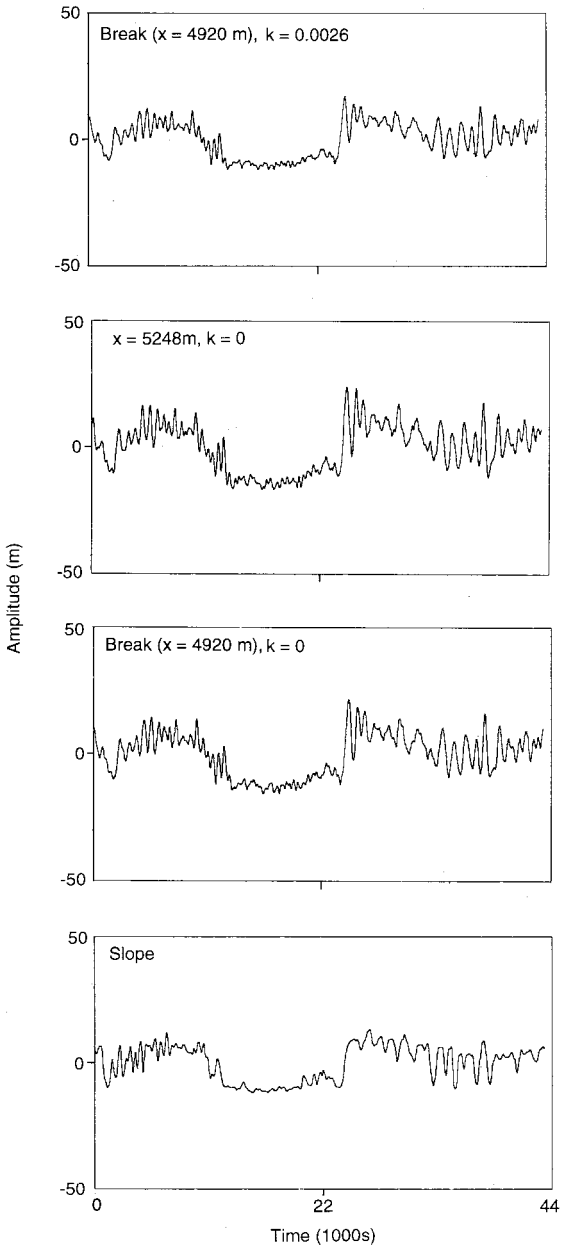

FIG. 20. Numerical simulation of wave transformation using the waveform at the slope as the inital waveform. Predicted waveforms near the break ($x = 4920$ m) are shown for $k = 0$ and $k = 0.0026$ and at $x = 5248$ m for $k = 0$. Data are from 13 April 1992.

nonlinear steepening of the internal tide and formation of the ''back'' shock then the ''forward'' shock occur at approximately the same distances as calculated without bottom friction (this result also follows from the theoretical model within the nonlinear theory of long waves for the fluid of constant depth described by Klevanny and Pelinovsky 1977). The rate of growth in amplitude of the internal tide is less when bottom friction is included. Halving the coefficient of bottom friction ($k = 0.0013$) increases the number of short-period waves and their amplitudes (Fig. 16). The inclusion of internal wave damping due to a turbulent boundary layer produces waveforms similar to the observations (section 7).

Model runs including bottom friction ($k = 0.0026$) are made for the case when the nonlinear coefficient is calculated from Levitus data (Fig. 17). Compared to results excluding dissipation (Fig. 11) it can be seen that the oscillations are weaker and the crest and trough of the internal tide become flattened. The wave amplitude is essentially unchanged in the process of the wave propagation. Therefore, taking a reasonable value for the coefficient of bottom friction, the applicability of the assumption of weak nonlinearity over large distances is demonstrated and provides a reasonable comparison with observed wave features. Comparing Figs. 15 and 17, it is seen that the different approximations for α strongly influence the short-period waves. This is also seen in results of the numerical simulation for the case when α is described by the lower curve in Fig. 8 ($\alpha < 0$); these results are presented in Fig. 18 for $k = 0.0026$.

Decreasing the initial wave amplitude influences how rapidly the nonlinearity and dissipation take effect. Figure 19 shows results with α calculated from data of 1995 and with $k = 0.0026$ and $a_0 = 20$ m. Compared to results without dissipation (Fig. 13), it can be seen that the dissipation decreases the number of short period waves and their amplitudes and also the amplitude of the long internal wave. Therefore, dissipation influences mainly the wave amplitude which, for the reasonable estimates of the bottom friction coefficient, is not significantly changed in the coastal zone. On the other hand, the process of nonlinear generation of short-period waves occurs with or without the effects of bottom friction, and this process is sensitive to horizontal variability of α on the shelf/slope region.

7. Comparison with observations

For a more detailed comparison of the numerical simulations with observed data, consideration is made of simultaneous measurements of isotherm oscillations at the slope, break, and shelf locations. Isotherm displacements, over a 12-h period, observed at the slope location are used as the initial waveform, and the K-dV model is used to predict the wave transformation as it propagates to the break and then to the shelf locations. For the first example, isotherm displacements from 0000 to 1200 on 13 April (Fig. 3d) are used. Background vertical profiles of the density and shear flow fields and the corresponding coefficients of the K-dV equation are obtained by averaging the observed data from the slope over the 12-h period 0000 to 1200. In the first instance, simultaneous records are considered from the break and shelf. Second, a time shift related with the phase speed of internal waves (about 0.4 m s^{-1}) is considered and the averaging is carried out for the time interval 0300–1500 for the two inshore locations. The calculated val-

Unauthenticated | Downloaded 09/25/22 05:48 AM UTC

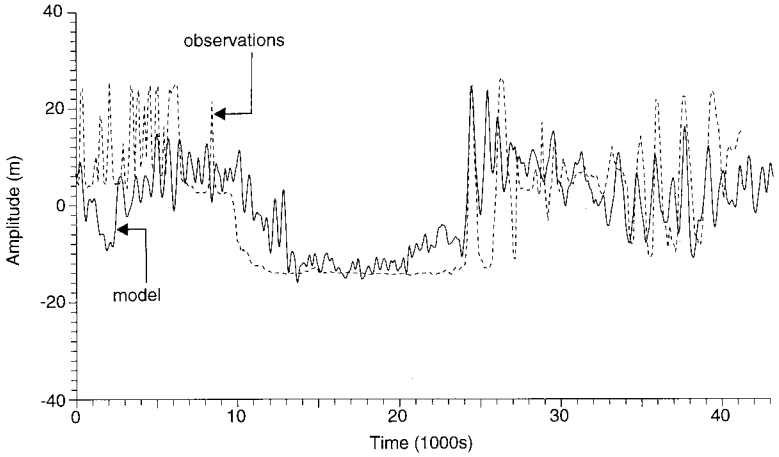

FIG. 21. Comparison of predicted waveform, calculated with $k = 0$, with observed isotherm displacements at break ($x = 4920$ m) on 13 April 1992.

ues of the coefficients of the K-dV equation in both cases are the same at the break and only slightly different at the shelf (Table 4). Between the locations the coefficients are approximated by a cubic spline.

The predicted waveforms near the break (after the initial wave has propagated 4920 m) and approaching the shelf (after propagating 5248 m) for different values of the bottom friction coefficient are shown in Fig. 20. The waveforms at the break with $k = 0$ and $k = 0.0026$ are similar, the main difference being in the amplitudes of the short-period waves. The greatest change in the waveform between the slope and break is the strengthening of the ''forward'' shock, formed from the positive sign of α, and an increase in amplitude of the short-period waves. With further propagation toward the shelf, the shock increases in strength and a large number of oscillations are seen. Simulations near the shelf need a large number of very short grid steps to resolve the short waves occuring at this location and, hence, large computing resources. Results of comparison between the observed and modeled waveforms are shown in Fig. 21 for $k = 0$ at the break, also see Fig. 3d. It can be seen that the theoretical model describes the low-frequency component and front shock correctly. Simulations predict the correct values of periods of short waves and their locations. There are differences between predicted and observed amplitudes of the short wave tail. The difference can be related with limitations of the theory, which is valid for relatively small amplitude waves, and using constant values of coefficients of K-dV equations (over 12 h). However, the agreement between theory and observations is reasonable. Note that even the short period oscillations in the observations, with periods of 8 to 10 min, are well resolved by the 2-min sampling interval used in collection of the data.

A second example of wave evolution is for the observed waveform at the slope over the period 1700 27 March to 0500 28 March 1992 (Fig. 3a). In this case there is strong variability in the nonlinear coefficient, calculated from 12-h average data (Table 5). The nonlinear coefficient calculated with no time shift is positive and increases in value between the slope and the break, decreasing again to the shelf, while when calculated with a time shift, α changes sign and becomes negative from slope to break and positive again to shelf. This demonstrates large temporal variability of α over a wave period and it is a limitation for comparison between theory and observations where the model assumes α is constant in time.

Results of the numerical simulation for both variants of computed coefficients α, β, and c, with $k = 0.0026$, are shown in Fig. 22. The forward shock is stronger for the first case (no time shift) because the nonlinearity is stronger. Also, amplitudes of the short-period waves generated on the shock front are larger. For the second case, α changes sign between the slope and the break and a weaker shock with a negative soliton forms. A comparison of the calculated and observed waveform

TABLE 5. The averaged values of coefficients of the K-dV equation for 12-h data segments during 27–28 March 1992. Two different averaging periods are considered.

	1700 27 Mar–0500 28 Mar			2100 27 Mar–0900 28 Mar		
Location	α	β	c	α	β	c
Slope	1.43×10^{-3}	89	0.34	—	—	—
Break	3.08×10^{-3}	65.7	0.24	-0.031×10^{-3}	55.5	0.24
Shelf	1.43×10^{-3}	89.1	0.22	1.24×10^{-3}	81.8	0.22

Unauthenticated | Downloaded 09/25/22 05:48 AM UTC

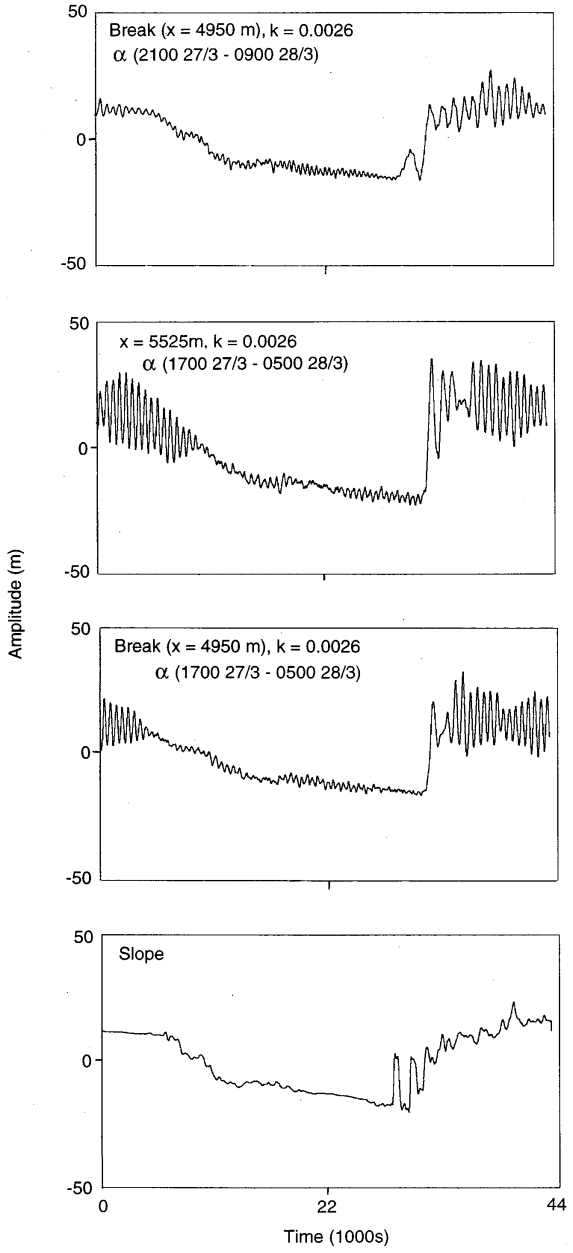

FIG. 22. Numerical simulation of wave transformation using the waveform at the slope as the inital waveform. Predicted waveforms near the break ($x = 4950$ m) are shown for $k = 0.0026$ and with α calculated as an average over the period 1700 27 March to 0500 28 March and from 2100 27 March to 0900 28 March, and at $x = 5525$ m for $k = 0.0026$. Data is from 27 to 28 March 1992.

at the break is presented in Fig. 23. It can be seen that the observed forward shock and following undulations are well described by the numerical simulation, although the model oscillations are stronger than observed. The agreement for the observed back shock is not as good. This back shock could possibly be explained by the model if the quadratic nonlinearity is very small (as in the second case with coefficients calculated with a time shift). In this case the cubic nonlinearity (second term in the asymptotic series on the wave amplitude) can be important. An analysis of effects related with the cubic nonlinearity, which can be significant only for rare cases of small quadratic nonlinearity, is out of the scope of this paper, but it is known that the ''cubic'' K-dV equation for internal waves (without quadratic nonlinearity) has steady state aperiodic solutions in the form of dissipation-free ''shock waves,'' which can occur as a forward shock and a back shock (see, e.g., Ostrovsky and Stepanyants 1989). The observed waveform in Fig. 23 is similar to the superposition of two steady-state aperiodic waves (known as the kink–antikink pair), but it is difficult to give a more detailed comparison taking into account the temporal variability of α in the generalized K-dV equation.

The analysis presented indicates that in the situation when the hydrological parameters of the ocean medium are stable, the numerical simulation is in good agreement with the observed data. However, α in the coastal zone exhibits large temporal and spatial variability and this limits the success of the developed model.

8. Conclusions

For a description of the nonlinear transformation of the internal tide on the NWS a theoretical model based on the generalized K-dV equation is developed. The model takes into account nonlinear and dispersive properties of the internal wave field and wave damping due to turbulent bottom friction. From a theoretical point of view, the model is valid to first order in wave amplitude and for long waves in a weak viscous fluid with a smooth horizontal inhomogeneity of the ocean medium. No account is made of the earth's rotation.

Coefficients of the generalized K-dV equation are calculated from background stratification and shear flow. The coefficients are calculated from climatic data (the Levitus atlas), from CTD observations from 1995, and from moored data in 1992 that include background shear flow. It is shown that for depths greater than 200 m all stratification data give similar values of the coefficients of the K-dV equation. It is expected that in deep water the background shear flow can be ignored, although no data were available to confirm this. For shallow water the variability of the nonlinear coefficient becomes large due to both the temporal variability of the density stratification caused by the large amptitude of the internal tide and due to the influence of the background shear flow, and this has a significant influence on the solution of the K-dV model. The change in sign of α along the path of wave propagation has previously been considered theoretically in the literature, but not previously confirmed by observations. Other coefficients (the phase speed c, the dispersion parameter β, the amplification factor P) are only weakly dependent on the variability in stratification and shear flow and can, with an accuracy of 30%, be calculated from climatic data.

Unauthenticated | Downloaded 09/25/22 05:48 AM UTC

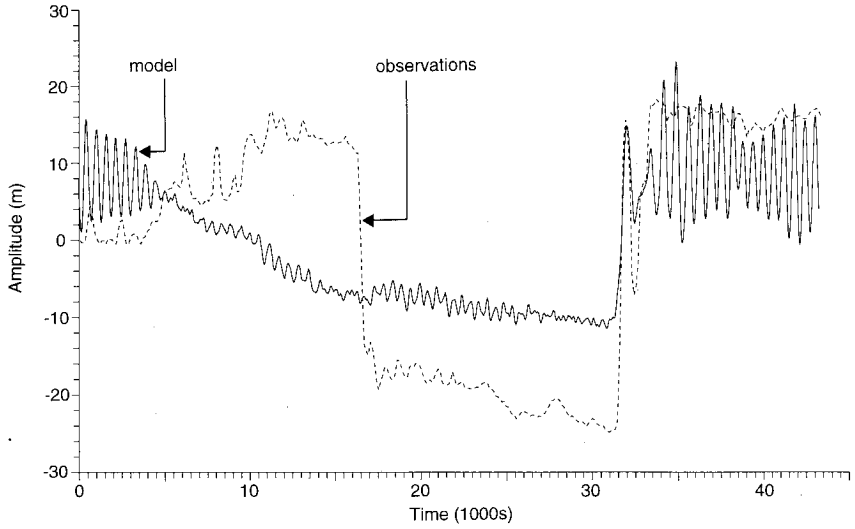

FIG. 23. Comparison of predicted waveform, calculated with $k = 0.0026$, with observed isotherm displacements at the break ($x = 4950$ m) on 27–28 March 1992.

A finite difference scheme for the generalized K-dV equation is proposed and the model is used for the numerical simulation of possible scenarios of the internal tide transformation on the NWS. The simulations show that the change in sign of α leads to interesting features in the dynamics of internal tide: shock formation on the back and forward fronts; generation of soliton groups of depression and their disintegration; generation of soliton groups of elevation; nonregular variation of short-period waves along the long internal tide. The results of calculations also show that a nondissipative model gives a significant amplification of wave amplitudes (up to six times). Bottom friction parametrized by a Chezy law reduces the amplification of the internal wave but only weakly in the shallow outer shelf. The model is sensitive to the spatial and temporal variability of α for the region of shallow depths (100 m) and this variability influences the number and amplitude of the short-period waves along the internal tide.

The main limitation for comparison with observed records of internal waves is due to the large temporal variability in the background stratification and shear flow. In the case when the background parameters of the ocean medium are stable, numerical simulation leads to good agreement with observed data. A number of records of the internal tide showing shocks on both the forward and back faces of the wave could be interpreted by taking into account the cubic nonlinearity, but here the temporal variability of α is high and this is not accounted for in the model.

Acknowledgments. Financial support for TT and EP to work in Australia was provided by a Bilateral Science and Technology grant. Two authors (EP and TT) have also been supported by the ISF Grant (N0S000) and the RFBR Grant (96-05-64108). Support for BB has been provided by an ARC Small Grant. The data from 1992 were collected under an ARC Large Grant in collaboration with PH, Ray Steedman, and Chris Fandry. The 1995 data were collected from R. V. Franklin by PH in collaboration with Peter Craig and Miles Furnas. The numerical scheme described in the paper was developed in collaboration with Yuri Stepanyants.

REFERENCES

Benney, D. J., 1966: Long nonlinear waves in fluid flows. *J. Math. Phys.,* **45,** 52–63.

Berezin, Yu. A., 1987: *Modelling Nonlinear Wave Processes.* VNU Science Press, 182 pp.

Boczar-Karakiewicz, B., J. L. Bona, and B. Pelchat, 1991: Interaction of internal waves with the seabed on continental shelves. *Contin. Shelf Res.,* **11,** 1181–1197.

Djordjevic, V. D., and L. G. Redekopp, 1978: The fission and disintegration of internal solitary waves moving over two-dimensional topography. *J. Phys. Oceanogr.,* **8,** 1016–1024.

Gallagher, B. S., and W. H. Munk, 1971: Tides in shallow water: Spectroscopy. *Tellus,* **23,** 4–5.

Gan, J., and R. G. Ingram, 1992: Internal hydraulics, solitons and associated mixing in a stratified sound. *J. Geophys. Res.,* **97C,** 9669–9688.

Gear, J. A., and R. Grimshaw, 1983: A second order theory for solitary waves in shallow fluids. *Phys. Fluids,* **26,** 14–29.

Goryachkin, Yu. N., V. A. Ivanov, and E. N. Pelinovsky, 1992: Transformation of internal tidal waves over the Guinean Shelf. *Sov. J. Phys. Oceanogr.,* **3**(4), 309–315.

Grimshaw, R., 1981: Evolution equations for nonlinear internal waves in stratified shear flows. *Stud. Appl. Math.,* **65,** 159–188.

——, 1983: Solitary waves in density stratified fluids. *Nonlinear Deformation Waves,* IUTAM Symp., Tallin, Springer, 432–447.

Halpern, D., 1971: Observations of short-period internal waves in Massachusetts Bay. *J. Mar. Res.,* **29,** 116–132.

Helfrich, K. R., W. K. Melville, and J. W. Miles, 1984: On interfacial solitary waves over slowly varying topography. *J. Fluid Mech.,* **149,** 305–317.

Holloway, P. E., 1984: On the semidiurnal internal tide at a shelf break location on the Australian North West Shelf. *J. Phys. Oceanogr.,* **14,** 1778–1790.

Unauthenticated | Downloaded 09/25/22 05:48 AM UTC

——, 1987: Internal hydraulic jumps and solitons at a shelf break region on the Australian North West Shelf. *J. Geophys. Res.,* **92,** 5405–5416.

——, 1994: Observations of internal tide propagation on the Australian North West Shelf. *J. Phys. Oceanogr.,* **24,** 1706–1716.

Huthnance, J. M., 1989: Internal tides and waves near the continental shelf edge. *Geophys. Fluid Dyn.,* **48,** 81–106.

Ivanov, V., E. Pelinovsky, Yu. Stepanyants, and T. Talipova, 1992: Statistical estimation of nonlinear internal long wave parameters from field measurements. *Izv. Atmos. Oceanic Phys.,* **28,** 794–798.

Jeans, D. R. G., 1995: Solitary internal waves in the ocean: A literature review completed as part of the internal waves contribution to Morena. Rep. U95-1, 64 pp. [Available from Unit for Coastal and Estuarine Studies, University College of North Wales, Marine Science Laboratories, Gwynedd, U.K.]

Klevanny, K. A., and E. N. Pelinovsky, 1978: Effect of nonlinear dissipation on the propagation of tsunamis. *Izv. Atmos. Oceanic Phys.,* **14,** 756–759.

Knickerbocker, C. J., and A. C. Newell, 1980: Internal solitary waves near a turning point. *Phys. Lett.,* **75A,** 326–330.

Lamb, K. G., 1994: Numerical experiments of internal wave generation by strong tidal flow across a finite amplitude bank edge. *J. Geophys. Res.,* **99,** 843–864.

Lee, C., and R. C. Beardsley, 1974: The generation of long nonlinear internal waves in a weakly stratified shear flow. *J. Geophys. Res.,* **79,** 453–462.

Levitus, S., 1982: *Climatological Atlas of the World Ocean.* NOAA Prof. Paper No. 13, U.S. Govt. Printing Office, 173 pp.

Liu, A. K., 1988: Analysis of nonlinear internal waves in the New York Bight. *J. Geophys. Res.,* **93**(12), 317–329.

——, J. R. Holbrook, and J. R. Apel, 1985: Nonlinear internal wave evolution in the Sulu Sea. *J. Phys. Oceanogr.,* **15,** 1613–1624.

Malomed, B., and V. Shrira, 1991: Soliton caustics. *Physica D,* **53,** 1–12.

Maslowe, S. A., and L. G. Redekopp, 1980: Long nonlinear waves in stratified shear flows. *J. Fluid Mech.,* **101,** 321–348.

Maxworthy, T., 1979: A note on the internal solitary waves produced by tidal flow over a three-dimensional ridge. *J. Geophys. Res.,* **84,** 338–346.

Miles, J. W., 1983: Solitary wave evolution over a gradual slope with turbulent friction. *J. Phys. Oceanogr.,* **13,** 551–553.

Morozov, E. G., 1995: Semidiurnal internal wave global field. *Deep-Sea Res.,* **42,** 135–148.

New, A. L., and R. D. Pingree, 1990: Large-amplitude internal soliton packets in the central Bay of Biscay. *Deep-Sea Res.,* **37A**(3), 513–524.

——, and ——, 1992: Local generation of internal soliton packets in the central Bay of Biscay. *Deep-Sea Res.,* **39A**(3), 1521–1534.

Ostrovsky, L. A., and Yu. A. Stepanyants, 1989: Do internal solitons exist in the ocean? *Rev. Geophys.,* **27,** 293–310.

Pelinovsky, E., and S. Shavratsky, 1976: Propagation of nonlinear internal waves in the inhomogeneous ocean. *Izv. Atmos. Oceanic Phys.,* **12,** 41–44.

——, and ——, 1977: Disintegration of cnoidal internal waves in a horizontally inhomogeneous ocean. *Izv. Atmos. Oceanic Phys.,* **13,** 455–456.

——, ——, and M. A. Raevsky, 1977: The Korteweg–de Vries equation for nonstationary internal waves in an inhomogeneous ocean. *Izv. Atmos. Oceanic Phys.,* **13,** 373–376.

——, Yu. A. Stepanyants, and T. G. Talipova, 1994: Modelling of the propagation of nonlinear internal waves in horizontally inhomogeneous ocean. *Izv. Atmos. Oceanic Phys.,* **30,** 79–85.

Sandstrom, H., and J. A. Elliot, 1984: Internal tide and solitons on the Scotian Shelf: A nutrient pump at work. *J. Geophys. Res.,* **89**(C4), 6415–6426.

——, and N. S. Oakey, 1995: Dissipation in internal tides and solitary waves. *J. Phys. Oceanogr.,* **25,** 604–614.

Smyth, N., 1988: Dissipative effects on the resonant flow of a stratified fluid over topography. *J. Fluid Mech.,* **192,** 287–312.

——, and P. Holloway, 1988: Hydraulic jump and undular bore formation on a shelf break. *J. Phys. Oceanogr.,* **18,** 947–962.

Voltsinger, N., K. Klevanny, and E. Pelinovsky, 1989: *Long-Wave Dynamics of the Coastal Zone* (in Russian). Gidrometeoisdat, Leningrad.

Zhou, X., and R. Grimshaw, 1989: The effect of variable currents on internal solitary waves. *Dyn. Atmos. Oceans,* **14,** 17–39.

Unauthenticated | Downloaded 09/25/22 05:48 AM UTC